Final Report

RETROFIT CATHODIC PROTECTION OF MARINE PIPELINES ASSOCIATED WITH PETROLEUM PRODUCTION

submitted to

Minerals Management Service
U.S. Department of the Interior
381 Elder Road
Herndon, Virginia 22070

by

William H. Hartt, Diane Lysogorski, Haijun Qian,
Keith Bethune, and Patrick Pierson,

Center for Marine Materials
Department of Ocean Engineering
Florida Atlantic University – Sea Tech Campus
101 North Beach Road
Dania Beach, Florida 33004

August 7, 2001

TECHNICAL SUMMARY

Marine oil and gas transportation pipelines have been in service in the Gulf of Mexico for almost 50 years. These lines are invariably protected from external corrosion by a combination of coatings and cathodic protection (cp); however, the design life of such protection systems upon older lines has now been exceeded in many cases such that some have required, and others will soon require, cp retrofitting. In response to this, the present project was initiated in 1997 for the purpose of establishing criteria and protocols for design of marine pipeline retrofit cp systems. Five research tasks were identified and addressed as:

I. Development of a New Approach to Cathodic Protection Design for New Marine Pipelines.

II. Development of An Inclusive, First Principles Based Attenuation Model for Marine Pipeline Cathodic Protection.

III. Verification of the Proposed Cathodic Protection Design Method and Attenuation Model.

IV. Definition and Examination of Critical Issues Related to Pipeline Cathodic Protection Retrofits.

V. Recommended Protocol for Retrofit Cathodic Protection Design of Marine Pipelines.

As background, a critical review and state-of-the-art summary for cp of petroleum production structures was conducted. This focused first upon cp of platforms, since the technology for these is more mature, and then proceeds to pipelines. Particular attention is given to the recent development of a unified, first-principles based design equation and cp design protocol termed the Slope Parameter Method. Within the above tasks, critical aspects of pipeline retrofit cp design have been identified; and it is demonstrated that the decision path and governing features for cp retrofits of pipelines are distinct from those associated with new construction. Specifically, Task IV identifies 1) determination of pipe cp current density demand, 2) optimization of retrofit anode array spacing, and 3) anode array design as particularly critical. Methods whereby Items 1 and 2 can be addressed are based upon the results from Tasks I and II, and Task III provides verification for these. The cornerstone of these efforts is, first, modification of the Unified Design Equation to pipelines and, second, development of a first-principles based potential attenuation and anode current output equation for pipelines. Protocol options for accomplishment of Item 3 (anode array design), on the other hand, are developed from the literature. Lastly, a flow chart that integrates these different cp design components is presented and discussed under Task V.

TABLE OF CONTENTS

1. EXECUTIVE SUMMARY ii
2. TABLE OF CONTENTS iii
3. NOMENCLATURE v
4. INTRODUCTION 1

General 1
Corrosion Control for Marine Pipelines 1
Aging Marine Pipeline Infrastructure 2
Cathodic Protection Design Protocol for Offshore Structures 3
General 3
Platforms 4
Pipelines 8
Corrosion and CP Assessment Methods 9
Existing Pipeline Cathodic Protection System Analysis Methods 10

5. PROJECT OBJECTIVES 13

6. TASK I: DEVELOPMENT OF A NEW APPROACH TO CATHODIC PROTECTION DESIGN FOR NEW PIPELINES 13

Development of Equations 13
Example Pipeline CP Design 16

7. TASK II: DEVELOPMENT OF AN INCLUSIVE, FIRST-PRINCIPLES BASED ATTENUATION MODEL FOR MARINE PIPELINE CATHODIC PROTECTION 17

General 17
The Governing Equation 17

8. TASK III: VERIFICATION OF THE PROPOSED CATHODIC PROTECTION DESIGN METHOD AND ATTENUATION MODEL 20

Attenuation Equation 20
Effect of Anode Spacing and Pipe Current Demand upon Potential Attenuation and Anode Current Output 24
Slope Parameter Method 27
Comparison with FDM Solutions 27
Range of Applicability of the Slope Parameter Design Approach 28

9. TASK IV: DEFINITION AND EXAMINATION OF CRITICAL ISSUES RELATED TO PIPELINE CATHODIC PROTECTION RETROFITS 30

Detection of pipeline Anode Expiration 30
Principle Design Parameters for Pipeline CP Retrofits 32
Pipeline Current Density Demand 33
Example Calculation of Pipe Current Density Demand 33
Anode/Anode Array Design 37
Maximized Anode/Anode Array Spacing 41

10. TASK V: RECOMMENDED PROTOCOL FOR RETROFIT CATHODIC PROTECTION DESIGN OF MARINE PIPELINES 50

11. BIBLIOGRAPHY 52

12. APPENDIX A: Derivation of the First-Principles Pipeline Attenuation Equation 54

13. APPENDIX B: Spacing Distance between Crossing Pipelines

NOMENCLATURE

A_a: Anode surface area.
A_c: Structure (cathode) surface area.
$A_{c(1)}$: Pipe surface area protected by a single anode.
C: Anode current capacity.
d: Distance from a offset anode to a position on a pipeline.
D: Diameter of a circle about with an array of equally spaced anodes are placed.
E_a: Magnitude of cathodic polarization at $z = 0$.
E_b: Magnitude of cathodic polarization at $z = L$.
$E_c(z)$: Magnitude of cathodic polarization at z.
f_c: Coating breakdown factor (fraction of the external pipe surface that is exposed at coating defects and bare areas).
i_o: Initial cathodic protection design current density.
i_m: Mean cathodic protection design current density.
i_f: Final cathodic protection design current density.
i_c: Structure (cathode) current density demand.
$i_c(z)$: Cathodic current density at z along a pipeline.
I_a: Current output of an individual anode.
$I_m(z)$: Metallic path current in a pipeline at z.
k: Polarization resistance of bare metal exposed at coating defects.
l: Length of an individual stand-off anode.
L: Half spacing between equally spaced anodes.
L_{as}: Anode spacing.
M: Total anode mass.
N: Number of galvanic anode.
OF: Distance from an offset anode and a pipeline
r: Anode radius or effective radius.
r_a: Equivalent radius of a spherical anode.
R_p: Pipeline radius.
R: Resistance.
$R(N)$: Resistance of an array of N anodes.
R_a: Resistance of an individual anode.
R_t: Total cathodic protection circuit resistance.
R_m: Pipeline metallic path resistance per unit length.
S: Distance between equally spaced anodes in a linear array.
S: Slope parameter.
S_a: Surface area of a cylindrical anode.
T: Cathodic protection system design life.
u: Anode utilization factor.
$U_m(z)$: Potential on the pipe side of the double layer.
$U_e(z)$: Electrolyte potential just outside the double layer.
v: Volume fraction of the anode that is galvanic metal as opposed to core.
w: Weight of an individual galvanic anode.
z: Distance along a pipeline from an anode.

a': Attenuation factor.
a: Polarization resistance.
f_a: Closed circuit anode potential.
f_c: Closed circuit cathode potential.
f_{corr}: Corrosion potential.
$f_c(z)$: Polarized pipe potential at z.
f_c(FF): Polarized pipe potential at large z.
f_c(Av): Average polarized pipe potential.
g: Ratio of total pipe surface area to bare surface area.

r': Anode density.
r_e: Electrolyte resistivity.
z: Coating resistance per unit length.

INTRODUCTION

General

There are in excess of 30,000 miles (48,000 km) of crude oil and gas marine pipelines in U.S. and state waters. While such pipelines are generally recognized as the safest, efficient, and cost effective means of transportation for offshore oil and gas from fixed production facilities, still failures occur because of 1) material and equipment problems, 2) operational errors, 3) corrosion, 4) storm/mud slides, and 5) third party incidents (mechanical damage). These, in turn, can result in loss of life, pollution, loss of product availability, repair expenses, business interruption, and litigation. Several publications (1-4) and a data base (5) have documented and evaluated the occurrence and causes of offshore pipeline failures that have taken place historically in the Gulf of Mexico and elsewhere. Each of these indicates that the major cause has been corrosion, with MMS data attributing over 50 percent of the failures to this mode. Of these, approximately 63 percent have occurred on pipelines as opposed to risers; and 69 percent resulted from external, as opposed to internal, corrosion. At the same time, however, only 12 percent of the external corrosion failures were on pipelines, with 88 percent being on risers. On the one hand, this indicates the susceptibility that prevails in the vicinity of the water surface, where corrosion rate is generally greatest. On the other, such failures are normally detected prior to substantial product discharge and are relatively inexpensive to repair. However, such data probably understates the role of corrosion, since instances where a pipeline has been weakened by corrosion but failed from an alternative cause (storm or third party damage, for example) are invariably attributed to the latter and not the former. Additional concerns with regard to pipeline corrosion failures are that, first, the average failure rate during the 1990's was more than double that of the 1980's; second, the increased focus in the Gulf of Mexico upon deep water production indicates that failures, where they occur, will be more difficult and expensive to address; and, third, the cathodic protection system design life for many older pipelines has now been exceeded such that external corrosion may be ongoing and cathodic protection retrofitting required. At the same time, no standardized procedure presently exists for design of retrofit cathodic protection systems for marine pipelines. Increased attention has, however, been directed in recent years toward this specific problem; that is, external corrosion of marine oil and gas pipelines, as evidenced by the fact that a 1991 International Workshop on Offshore Pipeline Safety (6) included only one paper that explicitly addressed corrosion and corrosion control; but a more recent MMS International Workshop (7) focused specifically upon this topic.

Corrosion Control for Marine Pipelines

Structural and high strength steels have historically been the only economically viable material for construction of marine petroleum transport pipelines. However, the inherent lack of corrosion resistance of this material class in sea water and the consequences of pipeline failure require that corrosion control

systems be designed, installed, and maintained such that a high degree of reliability is realized. Reliability considerations have become magnified in recent years with the transition from relatively shallow to deepwater installations. While cathodic protection (cp) has historically been employed as the sole corrosion control methodology for the submerged portion of petroleum production platforms, both mobile and fixed, the one-dimensional nature of pipelines is such that the combined use of coatings with cp is required. In the former case (platforms), anode resistance and structure current density demand are the fundamental parameters that are important in cp design. For pipelines, however, coating quality and metallic path (pipeline) resistance must also be taken into account, at least in the generalized case. Cathodic protection systems, either for pipelines or for other engineering applications, can be of either the impressed current (ic) or galvanic anode (ga) type. For marine pipelines, however, iccp systems are invariably limited to 1) proximity of landfall where protection can be provided seaward by a shore-based rectifier and anode array to a distance that is defined by the "throwing power" of the system and 2) pipeline runs between two platforms where the distance is sufficiently short that the entire line can be protected by a single rectifier and anode or anode template at one or both ends. In either case (shore or platform-based iccp), the limiting distance to which corrosion protection can be affected is normally limited by the voltage drop along the metallic pipeline that arises in conjunction with the current return to ground. An additional factor that affects the distance to which corrosion protection is afforded is quality of the protective coating. Thus, the higher the coating quality, the less the pipe current demand and, as a consequence, the less the voltage drop for a pipeline of a given length. However, coating quality of marine pipelines is invariably below that of buried onshore counterparts so that this distance of protection is considerably less in the former case than the latter. Also, coating quality, as defined by capacity of the coating to isolate the underlying steel, decreases with time; and, consequently, the distance to which protection is extended also becomes reduced. In order to maximize the distance to which protection is achieved, the region of the pipeline near the rectifier and anode array may be overprotected. Such overprotection can cause coating damage in the form of blistering and disbondment, in which case the pipe current demand increases. Because of these factors, corrosion control for the great majority of marine pipelines is provided by galvanic anodes (gacp); and for structural, economic, and installation considerations these are invariably of the bracelet type, as illustrated schematically in Figure 1. For these same reasons (structural and installation considerations) the size and, hence, weight of bracelet anodes is limited such that the spacing between anodes is, according to current practice, only about 750 feet (250 meters). Consequently, voltage drop in the pipeline is insignificant; and cp system life is governed by anode mass considerations alone.

Aging Marine Pipeline Infrastructure

Marine pipelines have been in service in the Gulf of Mexico since the 1940's. At the same time, cathodic protection systems for these are typically designed for 25-30 years. Consequently, the design life for the cp system of many older lines has been exceeded and for others is being approached. Also, earlier

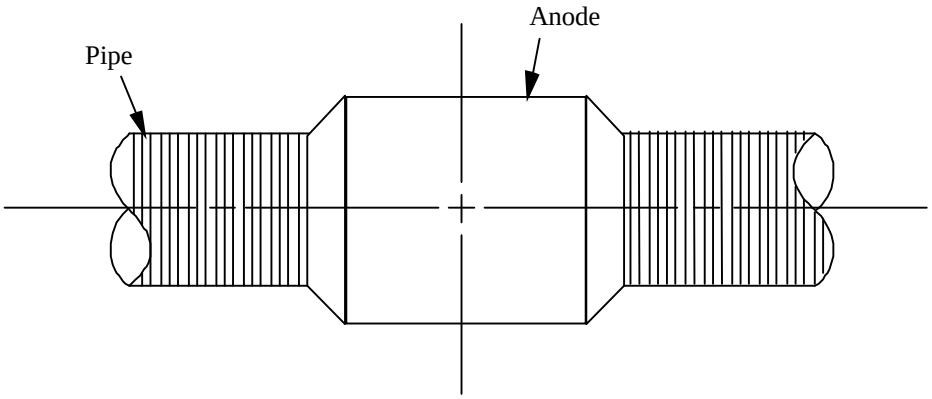

Figure 1: Schematic illustration of an offshore pipeline galvanic anode.

cp designs were typically less conservative than is the current practice; and anode quality was less. Thus, a one-quarter mile (400 m) bracelet anode spacing was commonly specified several decades ago. However, it is not uncommon for the electrical connection of an anode to the pipeline to become damaged or for the anode to become otherwise compromised during pipeline installation, which results in an effective doubling of the anode spacing. Deficient quality of anodes was invariably in the form of faulty chemistry, as can still occur today, such that 1) the pipeline failed to polarize, as explained below, or 2) anode consumption rate was high (low current capacity), or both. In either case (cp design life exceedance or lack of anode performance), external corrosion protection on older marine pipelines either may have been or is in the process of being lost. Consequently, pipeline cp retrofits have become increasingly common, both in the Gulf of Mexico and elsewhere; and the frequency of retrofits in the future is likely to become greater.

Cathodic Protection Design Protocol for Offshore Structures

General

It is generally recognized that corrosion of steel in sea water is arrested by polarization to a potential of –0.80 V_{AgCl} or more negative, and so achieving and maintaining a minimum polarization based upon this potential has been established as the goal of cathodic protection (8-10) irrespective of the type of structure involved (pipeline, platform, ship, and so on). Figure 2 illustrates schematically a pipeline with identical, equally spaced bracelet anodes and the resultant polarized potential profile. Thus, the pipeline is most polarized immediate to the anodes; and potential attenuates with increasing distance therefrom. Four factors determine the magnitude of this potential attenuation, as listed below:

1. Anode resistance. This resistance is encountered as current leaves the anode and enters the electrolyte. It is a consequence of the geometrical confinement in the vicinity of the anode. Accordingly, attenuation from this cause is greatest immediate to the anode and decreases with increasing distance. Anode resistance is higher the greater the electrolyte resistivity and the smaller the anode.

2. Coating resistance. The intrinsic resistivity of marine pipeline coatings is relatively high; however, coating defects and bare areas from handling, transportation, and installation are

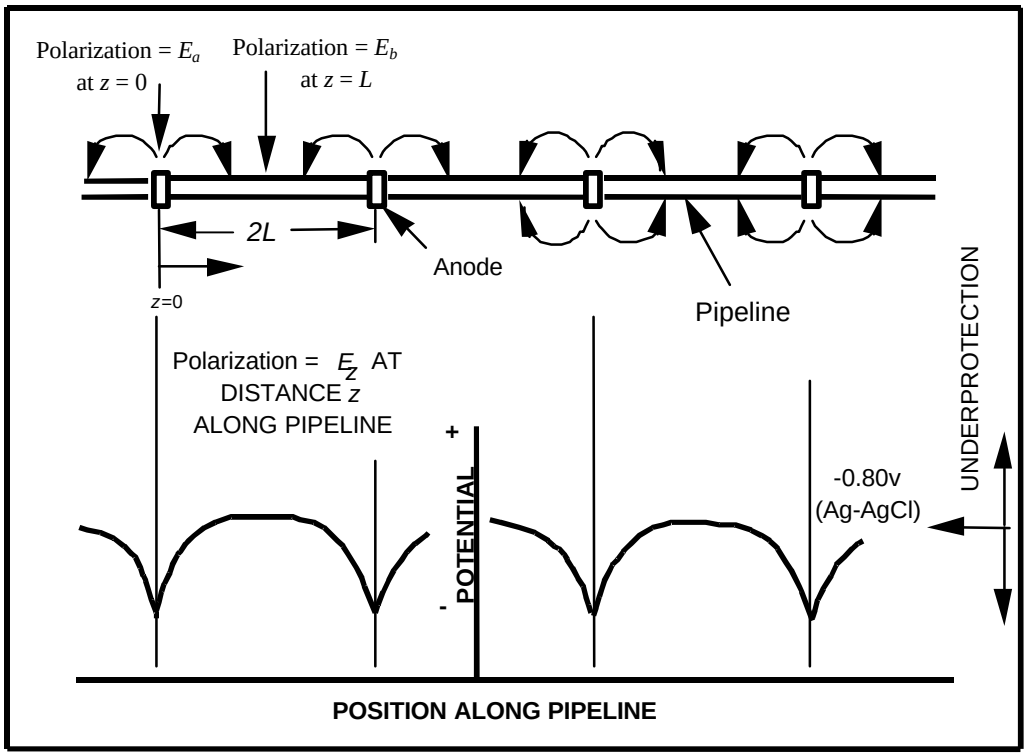

Figure 2: Schematic illustration of a cathodically polarized pipeline and the resultant potential profile.

invariably present. Consequently, the cp current enters the pipe at these locations where steel is directly exposed. Thus, the coating serves to reduce the exposed surface area of the pipeline compared to an uncoated situation, which, in turn, enhances the effectiveness, efficiency, and distance to which protection is achieved.

3. Polarization resistance. This resistance term reflects an inherent resistance associated with the cathodic electrochemical reaction whereby ionic current in the electrolyte is translated to electronic conduction in the pipeline.

4. Metallic resistance. Although resistivity of steel is orders of magnitude less that that of sea water, the confined pipeline cross section combined with the relatively long distance that current may have to travel in returning to electrical ground results in this term being influential, if not controlling, in some situations.

Portions of a pipeline for which potential is –0.80 V_{AgCl} or more negative are protected, whereas locations where potential is more positive are unprotected. Specific protocols that apply to cathodic protection design of platforms and pipelines are discussed below.

Platforms

Cathodic protection design procedures have evolved historically according to:

1. Trial and error.

2. Ohm's law employing a single, long-term current density (11).
3. Ohm's law and rapid polarization employing three design current densities, an initial (i_o), mean, (i_m), and final (i_f) (8,9).
4. The slope parameter method (12-15).

Accordingly, practices 2) and 3) are based upon the equation

$$I_a = \frac{f_c - f_a}{R_a}, \qquad (1$$

where

I_a = individual anode current output,
f_c = closed circuit cathode potential,
f_a = closed circuit anode potential, and
R_a = resistance of an individual anode.

As noted above, anode resistance is normally the dominant component of the total circuit resistance for space-frame structures such as platforms, and so it alone need be considered here. In most cases, this parameter is calculated from standard, numerical relationships that are available in the literature (16-21) based upon anode dimensions and electrolyte resistivity. Figure 3 graphically illustrates the principle behind this equation and approach.

Considering that the net current for protection, I_c, is the product of the structure current density demand (i_c) and surface area (A_c), the number of anodes required for protection, N, is determined from the relationship

$$N = \frac{i_c \cdot A_c}{I_a}. \qquad (2$$

By earlier practice (11), cp design was based upon a single, time average or mean current density that polarized the structure to the potential required for protection (-0.80 V_{AgCl}) within perhaps several months to one year. It was subsequently recognized, however, that application of an initially high current density (rapid polarization (21-26)) resulted in a lower mean current density and reduced anode mass to provide protection for the design life. Accordingly, present protocols (8,9) are based upon three current densities, an initial (i_o), mean (i_m), and final (i_f), where the first is relatively high and is realized upon initial deployment, the second is the time-averaged value, and the last reflects what is required near the end of the

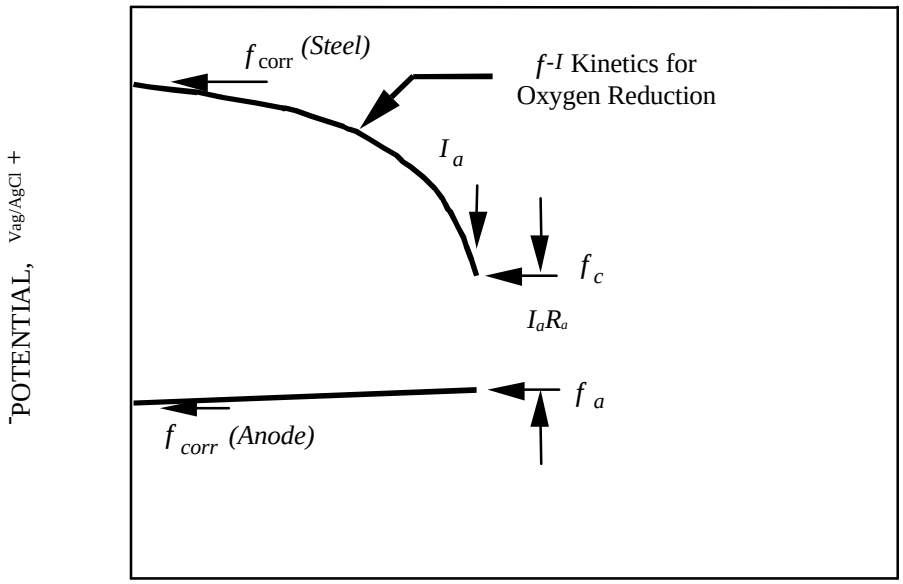

Figure 3: Schematic illustration of a polarization diagram and of parameters relevant to galvanic anode cathodic protection system design.

design life to affect repolarization should this become necessary. The required number of anodes corresponding to the respective values for i_o and i_f is determined by substituting each of these parameters for i_c in Equation 2. On the other hand, i_m is calculated from the mass balance relationship,

$$N = \frac{8{,}760 \cdot i_m \cdot A_c \cdot T}{u \cdot C \cdot w}, \qquad (3$$

where

T = design life of the cp system (years),
u = utilization factor (see Table 2),
C = anode current capacity ($\mathrm{A \cdot h/kg}$), and
w = weight of an individual anode (kg).

Invariably, the number of anodes determined according to each of the three calculations is different with the largest being specified. For uncoated structures this is usually i_o. Consequently, the system is over-designed in terms of the other two current densities. This arises because the procedure is an algorithm rather than being first principles based.

More recently, the slope parameter approach to galvanic cp system design (12-15) was developed

Table 2: typical anode utilization factors recommended for cp design (10).

Anode Type	Utilization Factor, unitless
Long[1] Slender Stand-Off	0.90
Long[1] Flush-Mounted	0.85
Short[2] Flush-Mounted	0.80
Bracelet, Half-Shell Type	0.80
Bracelet, Segmented Type	0.75

1. Anode length $\geq$ 4 x thickness.
2. Anode length < 4 x thickness.

based upon a modification of Equation 1 as,

$$f_c = (R_t \cdot A_c) \cdot i_c + f_a, \quad (4$$

where R_t is the total circuit resistance. This relationship projects a linear interdependence between f_c and i_c provided R_t, A_c, and f_a are constant. That this is normally the case has been confirmed by both laboratory and field measurements (12-15). For space frame type structures with multiple galvanic anodes,

$$R_t \cong \frac{R_a}{N}; \quad (5$$

with the product $R_t \cdot A_c$ (Equation 4) being defined as the slope parameter, *S*, such that,

$$S = \frac{R_a \cdot A_c}{N}. \quad (6$$

Substitution of the latter expression into Equation 4 then yields,

$$R_a \cdot w = \frac{i_m \cdot T \cdot S}{C}, \quad (7$$

which is referred to as the Unified Design Equation. Upon defining an appropriate value for *S*, all terms on the right side are known from the design choices. An anode type is then either selected or designed based upon the optimum combination of R_a and *w*. This may be accomplished in terms of anodes of standard dimensions or, perhaps more effectively, by specifying an elongated anode or dualnodes (27). Thus, if anode resistance is represented in terms of Dwight's modified equation,

$$R_a = \frac{r_e}{2pl} \cdot \left[ln\left(\frac{4l}{r}\right) - 1 \right], \quad (8$$

where

r_e = electrolyte resistivity,

l = anode length, and

r = equivalent anode radius,

then the left side of Equation 7 becomes

$$R_a \cdot w = \frac{r \cdot r' \cdot r^2 \cdot v}{2} \left[\ln \frac{4L}{r} - 1 \right], \quad (9$$

where

r' = anode density and

v = volume fraction of the anode that is galvanic metal as opposed to core.

The required number of anodes can then be calculated from Equation 6.

Hartt et al. (13) projected that the slope parameter based design approach yields a 32 percent reduction in anode mass in the case of typically sized structures compared to design according to present recommended practice 9,10). This arises because Equation 7 is first principles based and incorporates both i_m and i_o, the former explicitly and the latter implicitly via the slope parameter. As such, design can be optimized in terms of both parameters instead of just one. An alternative view is that, of the two terms on the left side of Equation 7, R_a determines i_o while w relates to i_m.

Pipelines

There are two fundamental differences between offshore platforms and pipelines: first, the three dimensional nature of the former compared to one dimensional for the latter and, second, the fact that pipelines are invariably coated while platforms are normally not. The same three design current densities, i_o, i_m, and i_f, are employed; however, marine pipeline cp design (9,10) considers the current demand, I_c, as

$$I_c = A_c \cdot f_c \cdot i_c, \quad (10$$

where f_c is the fraction of the external pipe surface that is exposed at coating defects and bare areas. Design values for i_o and i_f are normally in the range 5.6-20 mA/ft^2 (60-220 mA/m^2) (bare surface area basis)

depending upon pipe depth, temperature, sea water versus mud exposure, and whether or not the calculation is for the initial ($I_c = I_o$) or final ($I_c = I_f$) condition. As for platforms, the design is accomplished by substituting i_o and i_f for i_c and calculating the corresponding I_c. The net anode mass, M, on the other hand is determined from a modified form of Equation 3 as,

$$M = \frac{8{,}760 \cdot I_m \cdot T}{u \cdot C}, \qquad (11$$

where I_m is the mean current to protect the pipeline. The required number of anodes is then determined considering the values for I_o, I_f, and M. As noted above, the limiting feature of the pipeline cp design protocol is the maximum permissible anode bracelet size, as determined by structural and installation considerations. Because bracelet anodes are relatively small, so also is their spacing along the pipeline. This, in turn, results in metallic path resistance and voltage drop being negligible such that these need not be considered in the design. Consequently, this design method is not applicable to situations that call for maximizing anode or anode array spacing, as are likely to arise in the case of retrofit cp designs. This particular point is discussed in detail subsequently.

Corrosion and CP System Assessment Methods

The problem of marine pipelines becoming under-protected because of under-performance or expiration of the cp system anodes is compounded by the difficulty of characterizing the corrosion state. This is not the case for offshore platforms where a simplified potential survey (drop cell method) is performed annually and a comprehensive close interval survey at five year intervals. Here, the space frame nature of such structures is such that protection to a given region is normally provided by multiple anodes; and even if corrosion develops locally, it is likely to be of little consequence. For pipelines, on the other hand, 1) a single galvanic anode typically protects a specific line length, 2) localized corrosion, if undetected, can lead directly to failure, and 3) corrosion survey logistics are relatively complex. Because of the last point, present regulations specify only that measurements be made at locations of convenience, which are likely to be where the pipeline contacts a platform or pumping station. However, because such facilities are themselves cathodically protected and the pipeline may be in electrical contact with these, the pipeline may be protected here irrespective of the state of its own cp system. Protection may not be present, however, at more remote locations. Nonetheless, methods do exist and are practiced whereby over-the-line corrosion and cp assessment surveys are performed. These include the following:

1. Towed Vehicle/Trailing Wire Potential Measurements.
2. ROV Assisted Remote Electrode Potential Measurements.
3. ROV Assisted/Trailing Wire Potential Measurements.
4. Electric Field Gradient Measurements.

The first three are based upon pipeline potential measurements that are made either continuously or at closely spaced intervals along the line employing either a towed vehicle (method 1) or ROV (methods 2 and 3) upon which a reference electrode is mounted. Use of an ROV provides visual imaging and facilitates placement of the electrode close to the pipeline at locations where the line is not buried. In the towed vehicle case and where the pipe is buried, it must be assumed that the reference electrode is either "remote" or "semi-remote" to the pipeline, in which case only potential variations from long-line effects are disclosed. For such situations, localized corrosion is not likely to be detected. Figure 4 schematically illustrates a pipeline with a galvanic anode and the resultant potential profile. Thus, potential is relatively negative at the anode and positive at coating defects on the pipeline. As indicated, however, the profile that is measured becomes relatively flat as distance of the reference electrode from the pipeline increases. Consequently, a sufficiently remote electrode will not disclose presence of coating defects and any associated localized under-protection. The electric field gradient (EFG) method, on the other hand, utilizes two or more electrodes and is based upon the principle that the potential difference between these is proportional to the current that flows 1) into a pipeline at coating defects or 2) outward from anodes. The sensitivity of this method exceeds that of the other three, provided the electrodes can be positioned sufficiently close to the pipeline, in that the location and severity of coating defects and, with appropriate instrumentation and analysis, current output of anodes can be determined (28).

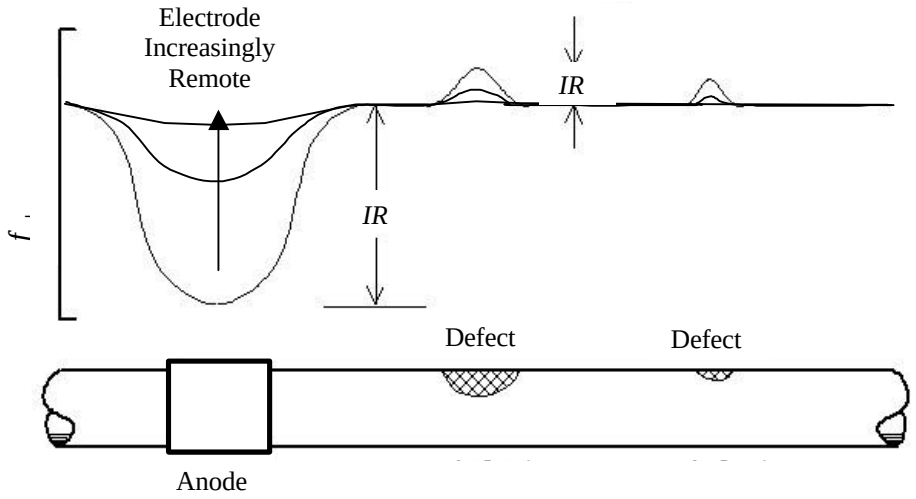

Figure 4: Schematic illustration of a pipeline and the potential that is recorded for an over-the-line survey.

Existing Pipeline Cathodic Protection System Analysis Methods

The equations of Morgan (29) and Uhlig (30) have been employed historically to project 1) potential attenuation along a pipeline and 2) the current requirement to achieve the indicated level of polarization in terms of coating and pipe properties and pipe dimensions. Thus, Morgan reasoned that the current terms

associated with a cp anode conform to the model illustrated in Figure 5. Based upon these, he established a differential equation the solution of which is,

$$E_c(z) = E_b \cdot \cosh a'(L - z) \text{ and}$$
$$E_a = E_b \cdot \cosh(a' \cdot L), \quad (12$$

where E_z and E_b are defined in Figure 2 and a', the attenuation constant, equals $\sqrt{R_m / z}$ or the square root of the ratio of metallic pipeline to coating resistance per unit length (R and z, respectively). Further, on the basis that the design for an existing pipeline is adequate, such that protection is achieved, and that sufficient anode mass remains, the corresponding anode current output is

$$I_a = 2\left(\frac{2}{r_p}\right) a' \cdot E_b \cdot \sinh(a' L), \quad (13$$

where r_p is the pipe radius. On the basis of these assumptions, the current projected by this relationship constitutes the pipe current demand.

As a refinement to the pipeline potential attenuation equation of Morgan, Uhlig (30) proposed the relationships,

$$E_z = E_b \cdot \cosh\left[\left(\frac{2\pi r_p \cdot R_m}{k \cdot z}\right)^{1/2} \cdot (z - L)\right] \text{ and}$$
$$E_a = E_b \cdot \cosh\left[-\left(\frac{2\pi r_p \cdot R_m}{k \cdot z}\right)^{1/2} \cdot L\right], \quad (14$$

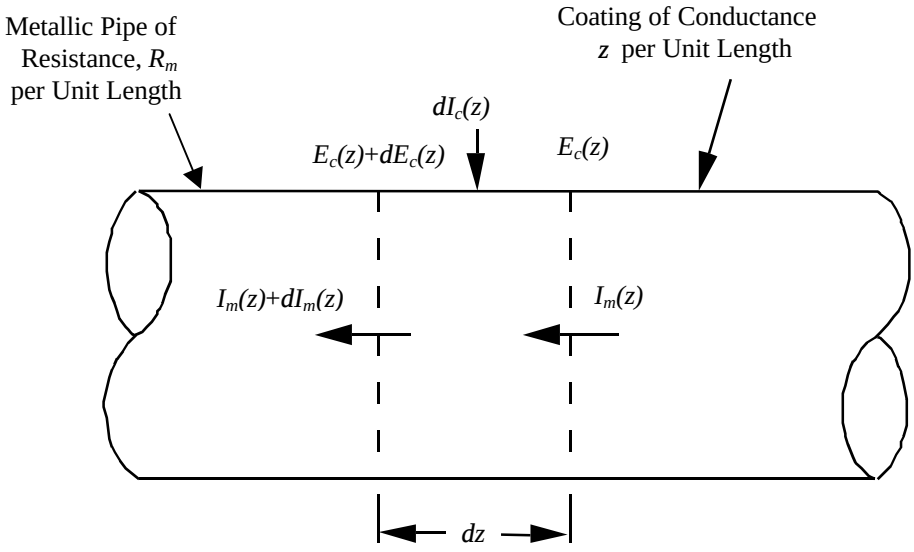

Figure 5: Current and potential in a cathodically polarized pipe element.

where k is a constant that reflects 1) polarization characteristics of bare metal exposed at the base of coating defects and 2) effective coating resistivity. Correspondingly, Uhlig's equation for anode current output is,

$$I_z = \left(\frac{2E_b}{R_m}\right)\cdot\left(\frac{2pr_p \cdot R_m}{k \cdot z}\right)^{1/2} \cdot sinh\left[\frac{z}{2}\cdot\left(\frac{2pr_p \cdot R_m}{k \cdot z}\right)^{1/2}\right], \qquad (15$$

where E_b is the pipe potential at $z = L$ (see Figure 2).

If, in addition to sufficient anode mass being present, the coating quality is good, then Equations 13 and 15 project potential attenuation to $z = L$ (the one-half anode spacing position or location where potential should be most positive) to be minimal (perhaps a few millivolts or less) provided anode spacing is not excessive. However, this attenuation should increase with time as anodes expire (current output per anode decreases) or the coating deteriorates (or both); and eventually the current demand of the pipeline exceeds the anode output capability. The onset of such potential attenuation is a fundamental indicator that a need for cp retrofit is eminent even though the pipeline may still be protected (E_z more negative than -0.80 V_{AgCl} everywhere along the line). However, the time frame during which this transition from protection to under-protection transpires may be relatively short compared to that for a jacket type structure, as addressed subsequently. A fundamental limitation of Equations 12-15 is that they consider only the coating and pipeline, but not anode, resistance terms. Consequently, an approach based upon these relations precludes 1) optimization of anode spacing and 2) evaluation of anode expiration and the onset of under-protection except in the special case where anode resistance is negligible. Also, the potential profile that is projected may by non-conservative (less protective) than is actually the case.

More recently, Boundary Element Modeling (BEM) has been applied to analysis of potential attenuation along pipelines and anode current output (31). This approach utilizes a numerical algorithm for the solution of a Laplace type governing equation,

$$\nabla^2 f = \frac{\partial^2 f}{\partial x^2} + \frac{\partial^2 f}{\partial y^2} + \frac{\partial^2 f}{\partial z^2} = 0\,, \qquad (16$$

that describes the potential variation in an electrolyte. To model an electrochemical process, the Laplace equation is used in conjunction with specified boundary conditions that portray the geometry and effects of electrical sources and sinks. However, while this approach incorporates the electrolyte and coating resistance terms, it excludes the metallic pipe path component. Consequently, it can provide no quantitative information relevant to optimization of anode or anode array (sled) spacing.

PROJECT OBJECTIVES

As noted above, oil and gas transportation pipelines have now been in service in shallow Gulf of Mexico waters for in excess of five decades. Because the design life of cp systems for marine pipelines is typically 25-30 years, the useful service life for many of these may have been reached or is being approached. At the same time, the technology for protecting marine pipelines from external corrosion has evolved such that it is now recognized that the criteria, approaches, and materials employed for earlier generation lines may not have been adequately conservative.

Additional concerns are, first, pipeline corrosion inspections are often neither sufficiently sensitive or sufficiently comprehensive to necessarily disclose problems and, second, pipelines may experience modified service conditions. The present project was initiated in 1997 with the objective of defining criteria and a standardized practice for retrofitting the cathodic protection system on older marine pipelines. Specific tasks that were addressed include the following:

I. Development of a New Approach to Cathodic Protection Design for New Marine Pipelines.

II. Development of An Inclusive, First Principles Based Attenuation Model for Marine Pipeline Cathodic Protection.

III. Verification of the Proposed Cathodic Protection Design Method and Attenuation Model.

IV. Definition and Examination of Critical Issues Related to Pipeline Cathodic Protection Retrofits.

V. Recommended Protocol for Retrofit Cathodic Protection Design of Marine Pipelines.

Each of these is discussed in the subsequent sections.

TASK I: DEVELOPMENT OF A NEW APPROACH TO CATHODIC PROTECTION DESIGN FOR NEW PIPELINES

Development of Equations

As a component of this project, a new approach to marine pipeline cp design was developed. Although this topic may appear to be outside the overall objective of this project, it is demonstrated subsequently to be relevant. The approach that was taken was to determine if the slope parameter approach to cp design of offshore structures (platforms or space frame structures) can be applied to pipelines. In this regard, application of Equation 4 to a coated, cathodically polarized pipeline requires that 1) spacing between anodes be sufficiently small that metallic path resistance is negligible, 2) pipe resistance to sea water is negligible, 3) all current enters the pipe at holidays in the coating (bare areas), and 4) f_c and f_a are constant with both time and position. As a consequence of 1) and 2), $R_t \cong R_a$; and from 3),

$$A_{c(1)} = \frac{2p \cdot r_p \cdot L_{as}}{g}, \qquad (17$$

where $A_{c(1)}$ is the pipe surface area protected by a single anode, g is the ratio of total pipe surface area to bare surface area (this parameter is a modification of the coating breakdown factor, f_c, that was introduced in conjunction with Equation 10), and L_{as} is the anode spacing or $2L$. Table 2 provides a comparison between g and the coating breakdown factor, f_c. Combining Equations 4 and 17 and solving for L_{as} then yields,

$$L_{as} = \frac{(f_c - f_a) \cdot g}{2p \cdot r_p \cdot R_a \cdot i_c}. \qquad (18$$

A reasonable approximation is that f_c and i_c exhibit a linear interdependence, as illustrated by Figure 5. Thus,

$$i_c = \frac{f_{corr} - f_c}{a}, \qquad (19$$

where f_{corr} is the free corrosion potential and a is the polarization resistance. Combining Equations 18 and 19 leads to an initial design expression for anode spacing as,

$$L_{as} = \frac{(f_c - f_a)}{f_{corr} - f_c} \cdot \frac{a \cdot g}{2p \cdot r_p \cdot R_a}; \qquad (20$$

Table 2: Correspondence of the Coating Breakdown Factor and g to the percentage of bare area and the corresponding $\alpha \cdot \gamma$ for a values of 20, 40, and 60 $\Omega \cdot m^2$.

BARE AREA, %	COATING BREAKDOWN FACTOR	g	ASSUMED a, $\Omega.m^2$	CORRESPONDING $a \cdot g$, $\Omega \cdot m^2$
0	0	∞	-	-
2	0.02	50	20 40 60	1,000 2,000 3,000
5	0.05	20	20 40	400 800
10	0.1	10	60 20 40 60	1,200 200 400 600
100	1	1	20 40 60	20 40 60

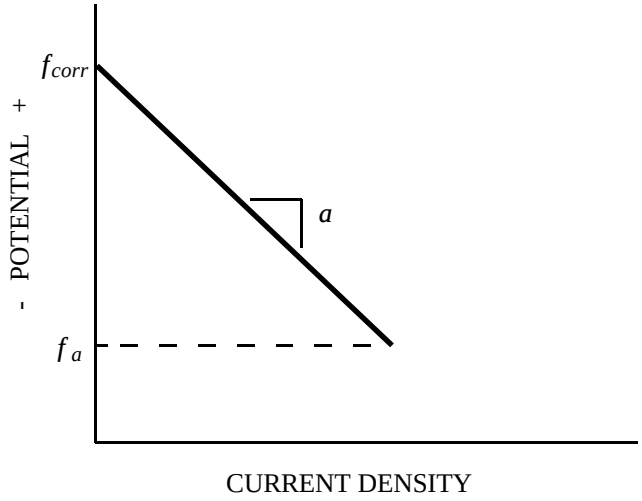

Figure 6: Proposed f_c versus i_c relationship with definition of a..

or, alternatively,

$$f_c = \frac{f_{corr} + (f_a \cdot y)}{1 + y}, \tag{21}$$

where

$$y = \frac{a \cdot g}{2p \cdot r_p \cdot L_{as} \cdot R_a}.$$

The corresponding design life can be calculated from the modified version of Equation 3,

$$T = \frac{w \cdot C \cdot u}{8{,}760 \cdot i_m \cdot A_{c(1)}}. \tag{22}$$

Finally, upon combining Equations 17, 19, and 22,

$$T = \frac{w \cdot C \cdot u \cdot a \cdot g}{8{,}760 \cdot (f_{corr} - f_c) \cdot 2p \cdot r_p \cdot L_{as}}. \tag{23}$$

Since the term $2p \cdot r_p \cdot L_{as} \cdot R_a / g$ (Equation 23) is equivalent to S (Equation 6), this approach is termed

the Slope Parameter Method for pipeline cp design. However, the magnitude of this slope parameter differs from that of bare steel (12-15) by a factor of 1/γ. On the basis that an upper limit of i_m for most pipeline cp designs is 7 mA/ft^2 (75 mA/m^2) at f_c = -0.80 $V_{Ag/AgCl}$, then $a \geq 2.0\ \Omega \cdot m^2$. Considering further a realistic upper limit for the coating breakdown factor as seven percent (g = 14.3) leads to a likely lower limit value for $a \cdot g$ of 30 $\Omega \cdot m^2$.

The initial step for a given design then is to calculate a baseline L_{as} in terms of $a \cdot g$, R_a (actually, anode surface area or dimensions using, for example, McCoy's formula (32)), and f_c (design cathode potential) using Equation 20. Upon substitution of this L_{as} into Equation 23 and possibly with iteration via Equation 21 (such iteration may be necessary since anode dimensions and w are interrelated and changes in these, in addition to changes in L_{as} and $a \cdot g$, result in a different f_c and T, as calculated by Equation 23), w and T are optimized.

Example Pipeline CP Design

Consider as an example the pipeline and cp design choices listed in Table 3. For these, and assuming 1) a standard 133 pound (60.8 kg) bracelet anode of length 1.42 ft (0.432 m) and outer radius 1.23 ft (0.187 m), f_c = -0.975 $V_{Ag/AgCl}$ (this constitutes a design polarized potential), and 3) R_a = 0.353 Ω as determined from McCoy's formula (32),

$$R_a = \frac{0.315 \cdot r_e}{\sqrt{A_a}}, \qquad (24$$

where A_a is the anode surface area, then Equation 20 indicates L_{as} = 170 m. From Equation 23, the corresponding life is 30.1 years, which is consistent with the design requirement (Table 3). If these values differ significantly, then iteration between Equations 20 and 23 based upon alternative choices for w (or R_a), a, g, or L_{as} (or for a combination of two or more of these terms) is required.

Table 3: Listing of pipe and electrolyte properties and design choices used in the example.

Pipeline Outer Radius, m	0.136
Pipeline Inner Radius, m	0.128
Electrolyte Resistivity, $\Omega \cdot m$	0.80
Alpha, $\Omega \cdot m^2$	7.5
Gamma	20
Design Life, years	30
Anode Current Capacity, Ah/kg	1,700
Anode Utilization Factor	0.8
Open Circuit Anode Potential, $V_{Ag/AgCl}$	-1.05

This proposed method is considered to be an improvement upon the existing pipeline cp design approach because, first, it is first principles based and not an algorithm as is the present method and, second, of the additional parameters that it incorporates. Verification of the accuracy is presented subsequently as is discussion demonstrating applicability of the equations upon which the approach is based to retrofit cp situations.

TASK II: DEVELOPMENT OF AN INCLUSIVE, FIRST RPINCIPLES BASED ATTENUATION MODEL FOR MARINE PIPELINE CATHODIC PROTECTION

General

Limitations of the existing methods for modeling and analyzing potential attenuation along cathodically polarized marine pipelines were discussed above. Briefly, these amount to the fact that the Morgan/Uhlig approach does not incorporate anode resistance, whereas Boundary Element Modeling excludes metallic path resistance. The newly proposed slope parameter based method for cp design for new pipelines that was described in the preceding section also excludes metallic path resistance. With this in mind, an attempt was made to derive a first principles based attenuation equation that incorporates all four resistance terms (anode, coating, polarization, and metallic path resistances). This is presented in the following section.

The Governing Equation

The approach considers that electrode (pipe) potential, $f_c(z)$, can be represented as the charge gradient associated with the double layer or,

$$f_c(z) = U_m(z) - U_e(z) + K_{ref} \,, \qquad (25$$

where $U_m(z)$ and $U_e(z)$ are the metallic and electrolyte potentials, respectively, and K_{ref} accounts for the fact that $f_c(z)$ must be measured relative to a reference potential (constant). Also,

$$E_c(z) = f_c(z) - f_{corr} \,, \qquad (26$$

where $E_c(z)$ is the magnitude of polarization. Further, upon taking the second derivative of Equations 25 and 26 and combining,

$$\frac{\partial^2 E_c}{\partial z^2} = \frac{\partial^2 U_m}{\partial z^2} - \frac{\partial^2 U_e}{\partial z^2} \,. \qquad (27$$

Expressions were then developed for each of the three component terms, E_c, U_m, and U_e, and their second derivatives, as described in the Appendix. These were substitution into Equation 27, which led to the governing equation,

$$\frac{\partial^2 E_c(z)}{\partial z^2} + \frac{\partial E_c(z)}{\partial z} \cdot H \cdot \left(\frac{1}{r_a} - \frac{1}{z} \right) + E_c(z) \cdot \left(\frac{2H}{z^2} - B \right) = 2H \cdot \frac{1}{z^3} \cdot \int_z^L E_c\left(z^*\right) dz^*, \qquad (28$$

where r_a is the radius of identical spherical anodes[1] that are superimposed upon the pipe at intervals of $2L$ and

$$H = \frac{r_e \cdot r_p}{ag} \text{ and}$$

$$B = \frac{R_m \cdot 2pr_p}{ag},$$

where r_e is electrolyte resistivity, The same linear relationship between f_c and i_c that was assumed in development of Equations 20 and 23 (Figure 6) was employed here also. Because there is no known solution to Equation 28, it must be solved numerically. This was done using an iterative, explicit finite difference scheme that was based upon the first and second derivatives in space (33). The former was represented by a backward finite difference given by,

$$\frac{dE}{dz} = \frac{E_i^{m+1} - E_{i-1}^{m+1}}{dz}, \qquad (29$$

and the latter by,

$$\frac{d^2 E}{dz^2} = \frac{E_{i+1}^{m} - 2E_i^{m+1} + E_{i-1}^{m+1}}{dz^2}. \qquad (30$$

The integral term on the right hand side of Equation 28 was approximated using a trapezoidal summation method as,

[1] For mathematical simplicity, the model is based upon a spherical anode. Justification for this assumption, given that actual anode are cylindrical bracelets is presented subsequently.

$$\int_{z}^{L}\int E(t)dt = \frac{dz}{2}\left[E_{i}^{m+1} + 2E_{i+1}^{m} + 2E_{i+2}^{m} \ldots\ldots + 2E_{N-1}^{m} + E_{N}^{m}\right]. \quad (31$$

Substituting Equations 29, 30, and 31 into 28 yields,

$$\frac{E_{i+1}^{m} - 2E_{i}^{m+1} + E_{i-1}^{m+1}}{dz^{2}} + \frac{E_{i}^{m+1} - E_{i-1}^{m+1}}{dz}\cdot\frac{H}{2}\left(\frac{1}{r_a} - \frac{1}{z}\right) + E_{i}^{m+1}\cdot\left(\frac{H}{z^{2}} - B\right) =$$

$$\frac{2H}{z^{3}}\cdot\frac{dz}{2}\cdot\left[E_{i}^{m+1} + 2E_{i+1}^{m} + 2E_{i+2}^{m} \ldots\ldots + 2E_{N-1}^{m} + E_{N}^{m}\right], \quad (32$$

which can be solved as,

$$E_{i}^{m+1} = \frac{\frac{H\cdot dz}{z_i^{3}}\cdot\left[\left(\sum_{j=1}^{n-1} 2E_{i+j}^{m}\right) + E_{n}^{m}\right] + \frac{E_{i-1}^{m+1}}{dz}\cdot H\left(\frac{1}{r_a} - \frac{1}{z_i}\right) - \frac{E_{i-1}^{m+1}}{dz^{2}} - \frac{E_{i+1}^{m}}{dz^{2}}}{\frac{-2}{dz^{2}} + \frac{H}{dz}\left(\frac{1}{r_a} - \frac{1}{z_i}\right) + \left(\frac{2H}{z^{2}} + B\right) - \frac{H\cdot dz}{z_i^{3}}}, \quad (33$$

where n is the number of elements of length z. Equation 33 provides an explicit means to calculate the cathode over-potential at each internal node for the next iteration step (m + 1) based on the present values (iteration step 'm') at the nodes and their neighbors. The equations,

$$E_c(z=0) = f_a - f_{corr} = E_a \quad (34$$

and

$$\left.\frac{dE_c(z)}{dz}\right| = 0, \quad (35$$

represent the boundary conditions at the end nodes; and the derivative boundary condition at the mid-anode spacing is characterized by,

$$E_{i=n}^{m+1} = \frac{4\cdot E_{i=n-1}^{m+1} - E_{i=n-2}^{m+1}}{3}. \quad (36$$

The element closest to the anode, $E_{i=1}$, is assigned the value given by Equation 34, such that $E_{i=1} = E_a$. As an initial estimate is necessary for every element discretizing the cathode, a value for E_a is also assigned to every element for the initial iteration step, m = 1. The iteration sequence was ended when the difference

between the root mean square value of the cathode over-potential for the present and previous iterations, ΔE_{rms}, became less than 10^{-9}.

True convergence of the model means that as *dz* approaches zero, the results from the finite difference technique approach the true solution. In reality, the true solution is not known and is difficult to measure in-situ; and so validity of the present model was judged based upon comparisons with an alternative modeling technique (BEM) under conditions where this was considered acurate, as presented subsequently.

TASK III: VERIFICATION OF THE PROPOSED CATHODIC PROTECTION DESIGN METHOD AND ATTENUATION MODEL

Attenuation Equation

Figure 7 presents a plot of pipe potential as a function of distance from an anode as determined by 1) Equation 14, 2) Boundary Element Modeling (BEM), and 3) the Finite Difference Method (FDM) solution of Equation 28 for $a \cdot g$ values of 4, 20, 100, and 1,000 $\Omega \cdot m^2$ (an $a \cdot g$ of 4 $\Omega \cdot m^2$ corresponds to a bare pipe with a current density demand of 100 mA/m^2 at –1.05 $V_{Ag/AgCl}$, whereas an $a \cdot g$ of 1,000 $\Omega \cdot m^2$

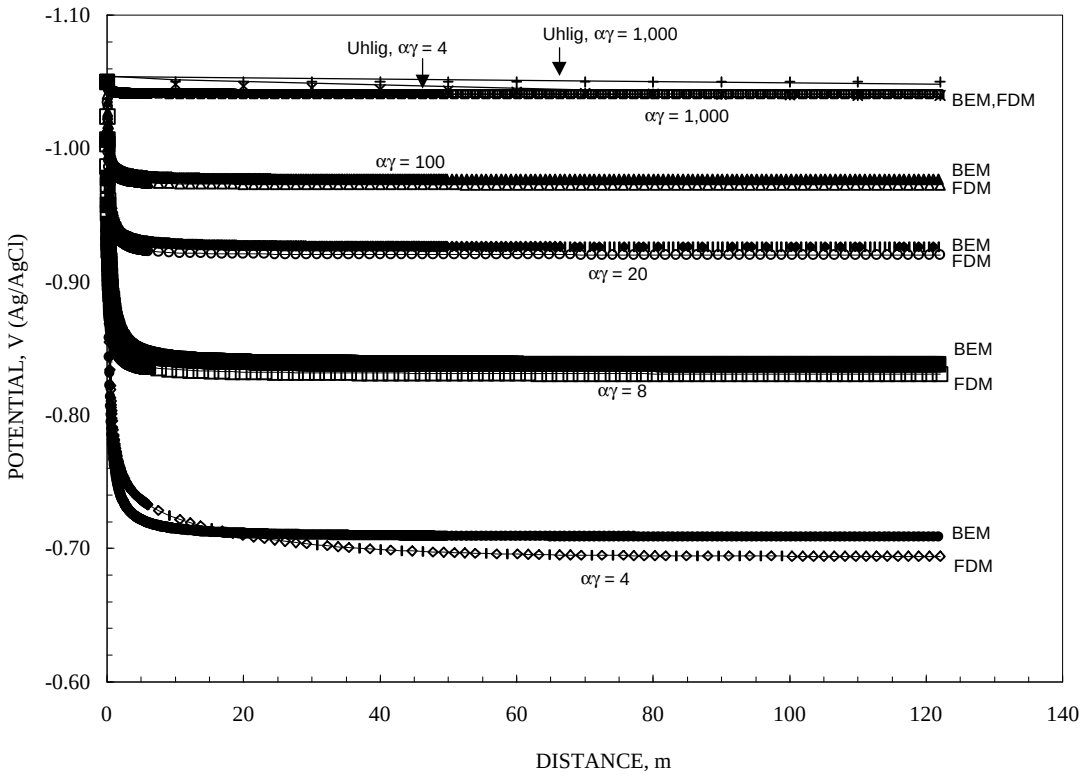

Figure 7: Potential as a function of distance for a pipeline protected by identical anodes spaced 244 m apart and with $a \cdot g$ values of 4, 8, 20, and 100 $\Omega \cdot m^2$.

corresponds, for example, to four percent bare area (g = 25) and a = 40 Ù·m^2 (current density demand of 10 mA/m^2 at –1.05 $V_{Ag/AgCl}$)). These $a \cdot g$ choices cover the range from a pipeline that is highly difficult to polarize ($a \cdot g$ of 4 Ù·m^2) to one that should be typical of what is encountered in practice ($a \cdot g$ of 1,000 Ù·m^2). Other pipe and electrolyte parameters are as listed in Table 4. For these conditions, the solutions to Equation 14 are relatively insensitive to coating quality and current density demand ($a \cdot g$) and are non-conservative compared to the BEM and Equation 28 results in that they predict greater cathodic polarization. The Equation 28 and BEM potential profiles, on the other hand, are in good mutual agreement. These are characterized by a potential decay within approximately the first 10 m of the anode, the magnitude of which is determined by 1) anode resistance (dimensions and electrolyte resistivity) and 2) the pipe current demand ($a \cdot g$). For each specific case, potential is relatively constant beyond the range where anode resistance is influential and is defined by the voltage drop associated with the anode. The finding that the FDM plateau potential is slightly more negative than the BEM one and that the magnitude of this difference is inversely related to $a \cdot g$ is probably due to inclusion of the metallic path

resistance term in the former solution and its exclusion in the latter. However, the difference in the two plateau potentials is not considered to be of practical significance. Because of the close correspondence between the BEM and FDM results and because BEM is a proven methodology for quantitatively characterizing potential fields, it is concluded that the FDM solution to Equation 28 is an appropriate means for projecting potential attenuation along pipelines and anode current output.

As a further confirmation, Figure 8 presents attenuation profiles from 1) BEM, 2) the FDM solution to Equation 28 with $r_m = 17 \cdot 10^{-8}\ \Omega \cdot m$ (the same as in Figure 7), and 3) the FDM solution to Equation 28 with r_m = 0 for the same anode and pipe dimensions as for Figure 7 and ag = 100 $\Omega \cdot m^2$ but for L = 3,000

Table 4: Pipe and electrolyte parameters for the analyses shown in Figure 7.

Pipeline Outer Radius, m	0.136
Pipeline Inner Radius, m	0.128
Anode Spacing, 2L, m	244
Equivalent Sphere Radius of Anode,[2] m	0.201
Electrolyte Resistivity, Ω·m	0.30
Pipe Resistivity, Ω·m	17x10^{-8}
Free Corrosion Pipe Potential, $V_{Ag/AgCl}$	-0.65
Anode Potential, $V_{Ag/AgCl}$	-1.05

[2] This size corresponds to that of a standard 133 pound (60.8 kg) bracelet aluminum anode.

m. The f_c versus z trend is characterized in each of the three cases by a relatively abrupt potential increase in the immediate vicinity of the anode that was apparent in Figure 7; but the FDM solution that includes the metallic path resistance term exhibits a further attenuation, albeit of a lesser magnitude, along the entire range of z, whereas the BEM and FDM solution that does not consider metallic path resistance exhibit an essentially constant potential in this same range. It is projected that the FDM solution with the finite metallic path resistance is the most accurate representation of the actual situation. On the other hand, it can be shown that Equation 28 reduces to the Uhlig expression for $R_a = 0$. Consequently, potential attenuation projected by BEM is non-conservative for situations where metallic path resistance is not negligible; and the Uhlig equation is non-conservative in cases where anode resistance is not negligible. It is concluded that Equation 28 provides a means for accurately assessing potential attenuation along a cathodically polarized pipeline and is likely to be the most accurate method for situations where both anode and pipe resistances are not negligible.

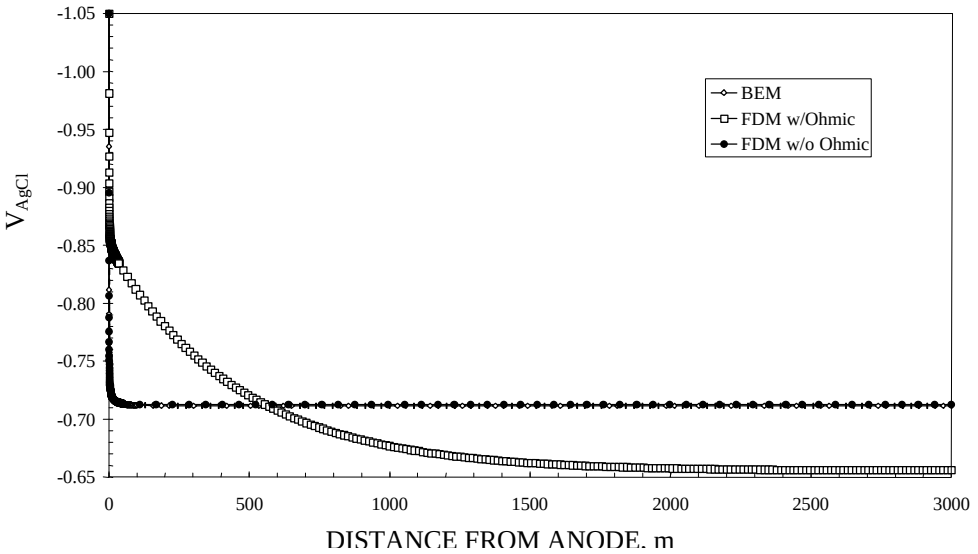

Figure 8: Comparison of BEM and FDM solutions to Equation 28 where the latter reflect presence and absence of the metallic path resistance term.

As noted above, Equation 28 was derived based upon the assumption that the anode is a sphere of radius r_a. However, marine pipeline anodes are typically of the "bracelet" type and, as such, have a cylindrical external surface as illustrated in Figure 1. A correction may be made for the difference between these two geometries using the same procedure that is employed in evaluating resistance of trapezoidal cross section stand-off anodes on space-frame structures in terms of Dwight's equation (16), as detailed in current recommended practices (8,9). In this regard, the approximate resistance to remote earth of a bracelet anode is typically calculated using McCoy's formula (Equation 24 (32)) modified as,

$$R_a \approx \frac{0.315 \cdot \rho}{\sqrt{S_a}}, \qquad (37$$

where S_a is the exposed surface area of a cylindrical anode. By equating the surface area of the bracelet anode to that of a sphere, the equivalent sphere radius, r_a is calculated as,

$$r_a \approx \sqrt{\frac{S_a}{4\pi}}\,. \qquad (38$$

Anode current output can be determined from both BEM and the FDM solution of Equation 28, since $E_c(z)$ is proportional to current demand which, in turn, dictates I_a. Thus, Figure 9 presents a plot of I_a versus ag, as determined by BEM, the FDM solution to Equation 28, and the Uhlig expression (Equation 14) based upon the same pipe and electrolyte parameters that were employed in conjunction with Figures 7 and 8. This reveals that results from the former two methods (BEM and FDM) are in excellent mutual agreement, whereas Uhlig's equation overestimates I_a in the lower ag range, presumably because of failure of this expression to adequately address the near-field and the greater influence of the near-field at relatively low ag. The Uhlig expression projects I_a with reasonable accuracy in cases where current demand and coating quality are such that $ag \geq 100\ \Omega \cdot m^2$. However, the BEM method is expected to overestimate I_a also for $2L$ values for which metallic resistance is no longer negligible.

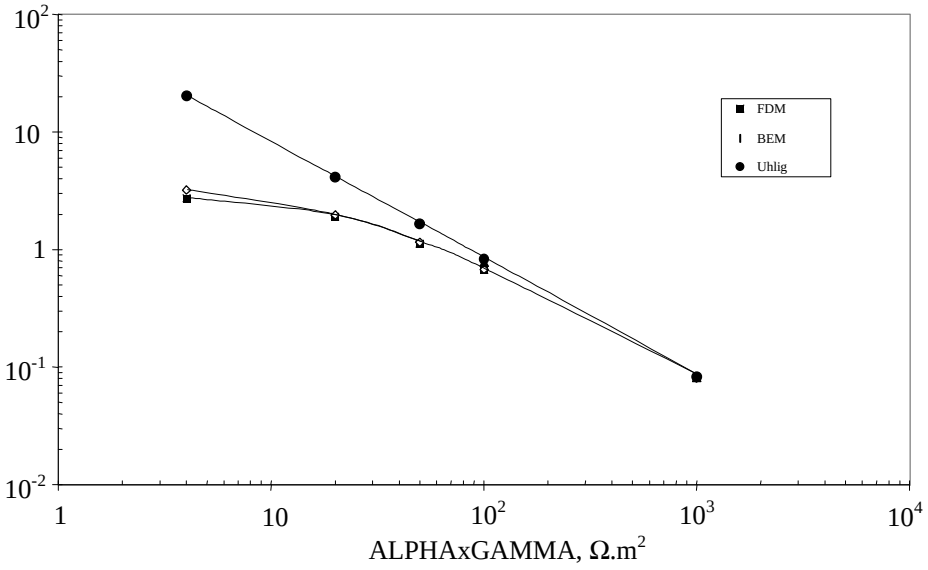

Figure 9: Comparison of anode current output as projected by BEM, FDM, and Equation 14.

The results in Figures 7 and 8 indicate that a FDM solution to Equation 28 provides an accurate projection of potential attenuation along a pipeline or riser and of anode current output. Because the equation incorporates the electrolyte (anode), coating, and metallic resistance terms, it represents an improvement over the Uhlig expression except in situations where electrolyte resistance is negligible and over BEM where metallic path resistance is non-negligible.

Effect of Anode Spacing and Pipe Current Density Demand upon Potential Attenuation and Anode Current Output

Figures 10 and 11 present attenuation profiles for different one-half anode spacings from 200 to 3,000 m and $a \cdot g$ =100 $\Omega \cdot m^2$ in the former case and for anode spacings from 100 to 10,000 m and $a \cdot g$ = 1,000 $\Omega \cdot m^2$ in the latter. The same pipe and environment parameters in Table 4 apply here as well. These plots

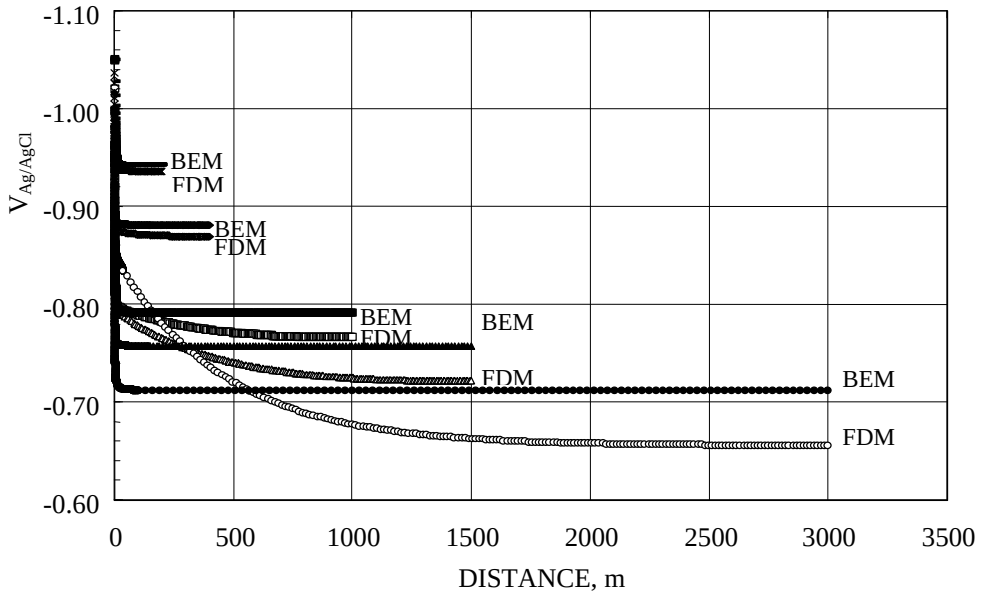

Figure 10: Comparison of BEM and FDM potential profiles for pipelines with anode spacings from 200 to 3,000 m and with $a \cdot g = 100\Omega \cdot m^2$.

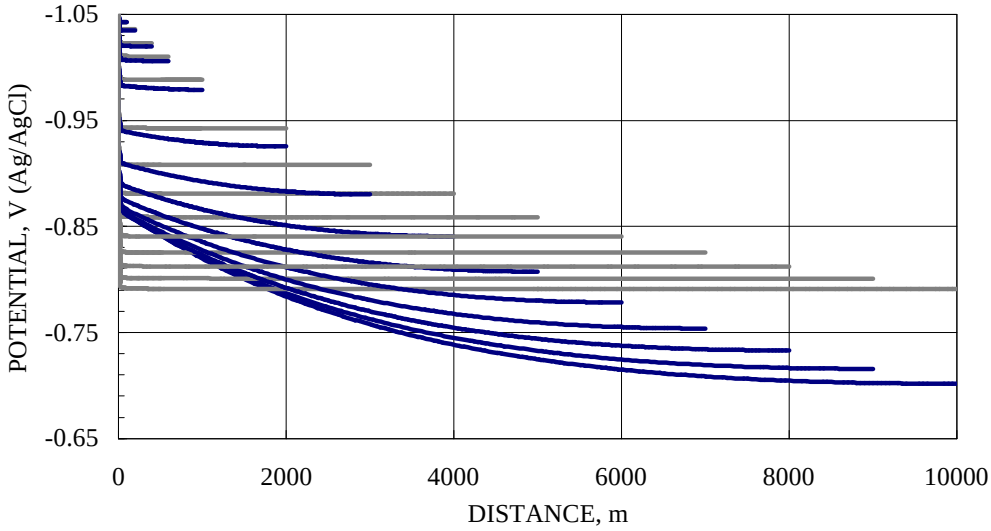

Figure 11: Comparison of BEM and FDM potential profiles for pipelines with anode spacings from 100 to 10,000 m and with $a \cdot g = 1{,}000\Omega \cdot m^2$. The more negative profile for each pipe length is the BEM solution and the more positive the FDM.

indicate that the difference between the two analysis methods (BEM and Equation 28) increases with 1) increasing distance from an anode, 2) increasing anode spacing, and 3) decreasing $a \cdot g$. The FDM solution is considered to be the more accurate of the two methods, at least for situations where metallic path resistance is non-negligible. On this basis, situations can arise where BEM indicates protection along the entirety of the pipeline but, in fact, under-protection exists beyond a certain distance. Accordingly, Equation 28 is recommended as the analysis method of choice.

Figures 12 and 13 show plots of anode current output as a function of one-half anode spacing for the same situations depicted in Figures 10 and 11, respectively. The BEM and FDM solutions are in good agreement for relatively short spacings, but for greater ones the former projects that this current increases

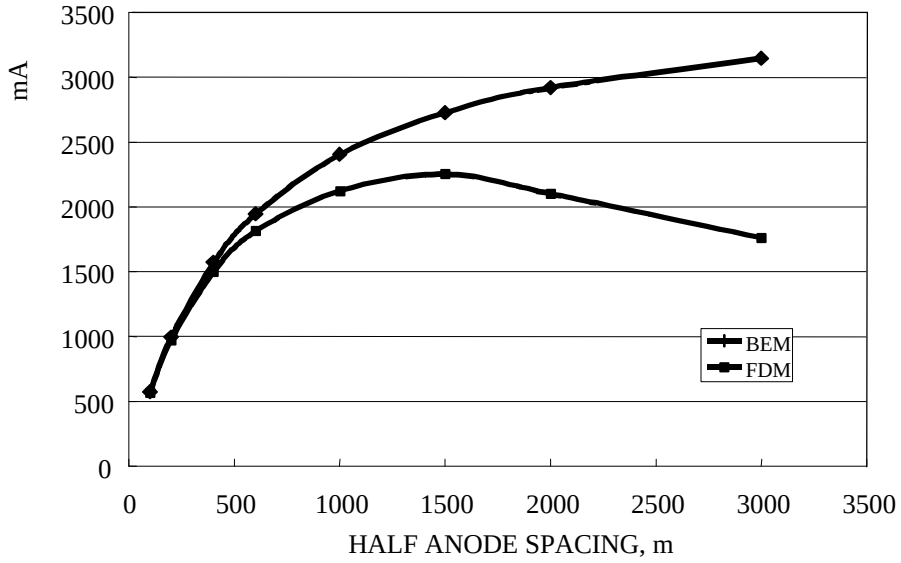

Figure 12: Anode current output, as projected by BEM and Equation 28 (FDM), as a function of half anode spacing and for $a \cdot g = 100\Omega \cdot m^2$.

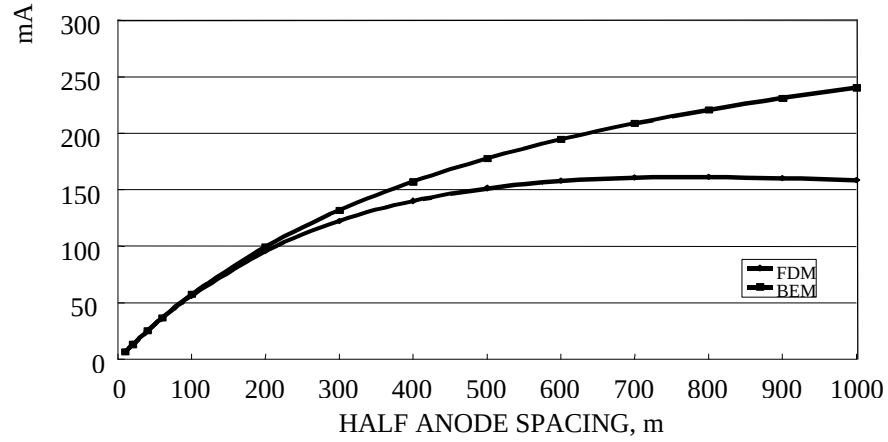

Figure 13: Anode current output, as projected by BEM and Equation 28 (FDM), as a function of half anode spacing and for $a \cdot g = 1{,}000\Omega \cdot m^2$.

progressively with increasing anode spacing whereas the FDM shows a maximum beyond which current decreases. The latter effect is more pronounced in the lower $\alpha \cdot g$ case. Again, this difference is apparently due to BEM not including the metallic path resistance term. Also, the situations in Figures 10 and 11, where a more positive potential is projected by FDM than by BEM, correspond to the lower anode current outputs in Figures 12 and 13.

Figure 14 presents a plot of potential difference between the BEM and the FDM solution to Equation 28, as shown graphically in Figures 10 and 11, at the mid-anode location as a function of $\alpha \cdot g$ and for various anode spacings from 50 to 10,000 m. This illustrates that, except for the shortest and greatest anode spacings (50 and 10,000 m, respectively), the difference between the two potentials increases with decreasing $\alpha \cdot g$. This is a consequence of I_a increasing with decreasing $\alpha \cdot g$ such that a correspondingly increasing voltage drop along the metallic path that was not accounted for in the BEM analysis resulted. This trend was absent in the $2L$ = 50 m case because metallic path resistance is negligible for such a short anode spacing at all $\alpha \cdot g$ values considered. A reverse trend resulted for $\alpha \cdot g$ values below about 600 $\Omega \cdot m^2$ and $2L$ = 10,000 m. This apparently occurred because for these conditions polarization at the mid-anode location was relatively small in both the FDM and BEM cases, and so the potential difference between the two was small also.

Figure 15 presents a plot of the percent difference in anode current output as a function of $\alpha \cdot g$ for

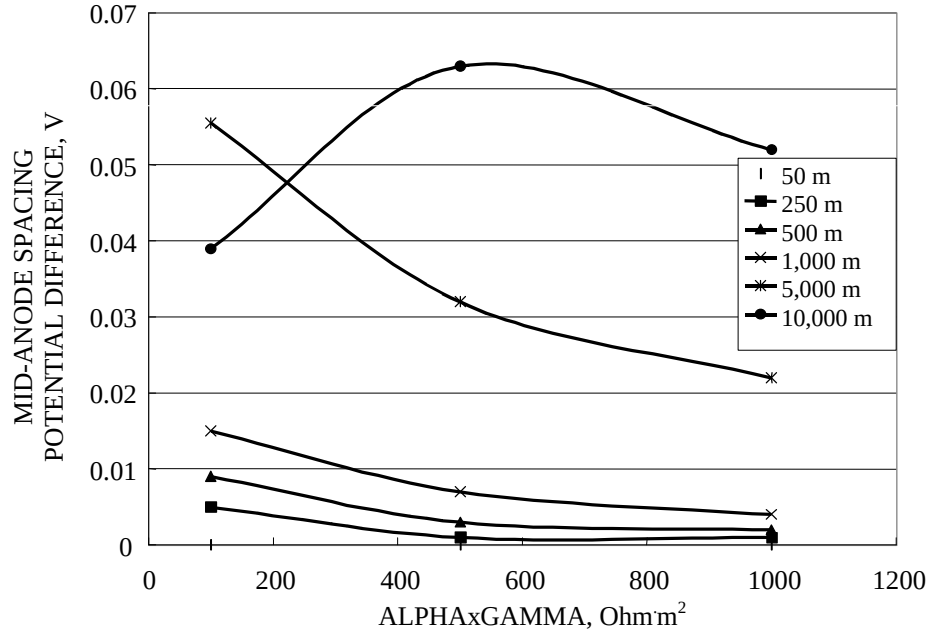

Figure 14: Plot of the difference between the FDM solution to Equation 28 and BEM projections of pipe potential at the mid-anode location for different anode spacings as a function of $\alpha \cdot g$. The convention employed was that a positive difference indicates a more negative projected potential via BEM.

the same $\alpha \cdot g$ values and anode spacings as in Figure 14. For 2*L* values of 1,000 m and below, the difference is seen to be by less that six percent in all cases. However, for the two largest anode spacings, the I_a projected by BEM was significantly greater than for the FDM solution to Equation 28, particularly at low $\alpha \cdot g$. In all cases, the difference increased with decreasing $\alpha \cdot g$. This trend is consistent with those in Figures 12 and 13, where the I_a values projected by the two methods diverge with increasing 2*L* with the effect being greater the lower the $\alpha \cdot g$.

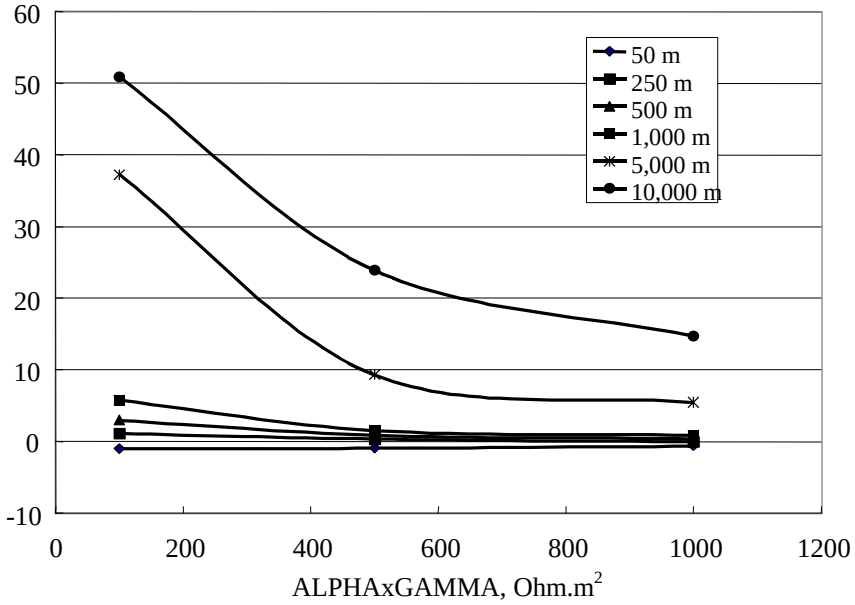

Figure 15 Plot of the percent difference in anode current output as projected by the FDM solution to Equation 28 and BEM for different anode spacings as a function of $\alpha \cdot g$. The convention employed was that a positive difference indicates that BEM projected greater I_a.

Slope Parameter Design Method

Comparison with FDM Solutions

Based upon Equation 28, a verification and qualification analysis was performed regarding accuracy of the Slope Parameter based method for pipeline cp design (Equations 20 and 23). Thus, Figure 16 shows the design f_c for both the original (assumed length 0.209 m and radius 0.160 m) and final (80 percent depleted) anode sizes, the former being –0.975 $V_{Ag/AgCl}$ by choice (L_{as} was calculated using this value) and the latter –0.943 $V_{Ag/AgCl}$ (determined by Equation 20 for f_c based upon L_{as} = 170 m and the final anode dimensions). Also illustrated are the attenuation profiles from a FDM solution of Equation 28. The two sets of potential profiles are seen to be in good agreement except in the immediate vicinity of the anode, as should be expected. The metallic path resistance can be considered negligible for this anode spacing and the $\alpha \cdot g$ considered ($100\,\Omega \cdot m^2$), since the trend demonstrated in Figures 10 and 11 (progressively more positive potential with increasing distance from an anode) is not seen in the FDM solutions in Figure 16. The difference in the profile pairs is attributed to failure of Equations 20 and 23 to take into account the

potential gradient near the anodes; however, this is thought to be within the uncertainty of the overall process; and, hence, the results are considered acceptable. Table 5 lists the anode current output determined by the two methods and indicates the difference to be relatively modest.

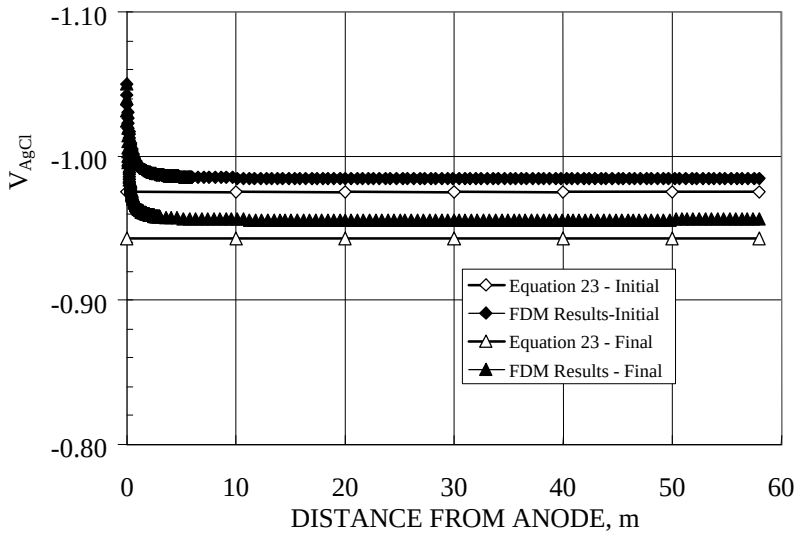

Figure 16: Comparison of the results from the FDM solution to Equation 28 with the cathode potential used in the cp design based upon Equation 23.

Table 5: Anode current output as determined using a modified version of Equation 22 and the solution to Equation 28.

Condition	Anode Current Output, A		Difference,
	Equation 22	FDM Solution	%
Initial (Anode Weight 60.8 kg)	0.214	0.221	-3.1
Final (Anode Weight 12.3 kg)	0.193	0.202	-4.4

Range of Applicability of the Slope Parameter Design Approach

The proposed cp design approach based upon Equations 20 and 23 was evaluated by comparing the results from it with the corresponding FDM solution to Equation 28. Thus, Figure 17 presents a plot of the percent difference in f_c at the mid-anode position (the location on the pipeline where polarization should be least) as a function of the corresponding $a \cdot g$ that results from application of Equation 20 compared to what is projected by the FDM solution to Equation 28 for the original anode and pipe dimensions in the above example using different values of L_{as}, and with r_e = 1.0 Ω·m. Only data for which $a \cdot g \geq 30$ Ω·m^2 and $f_c \leq$ -0.80 $V_{Ag/AgCl}$ are included. In all cases, the error is less than three percent; and so any design that includes the L_{as} and $a \cdot g$ values indicated here and which also satisfies Equation 22 or 23 is considered acceptable.

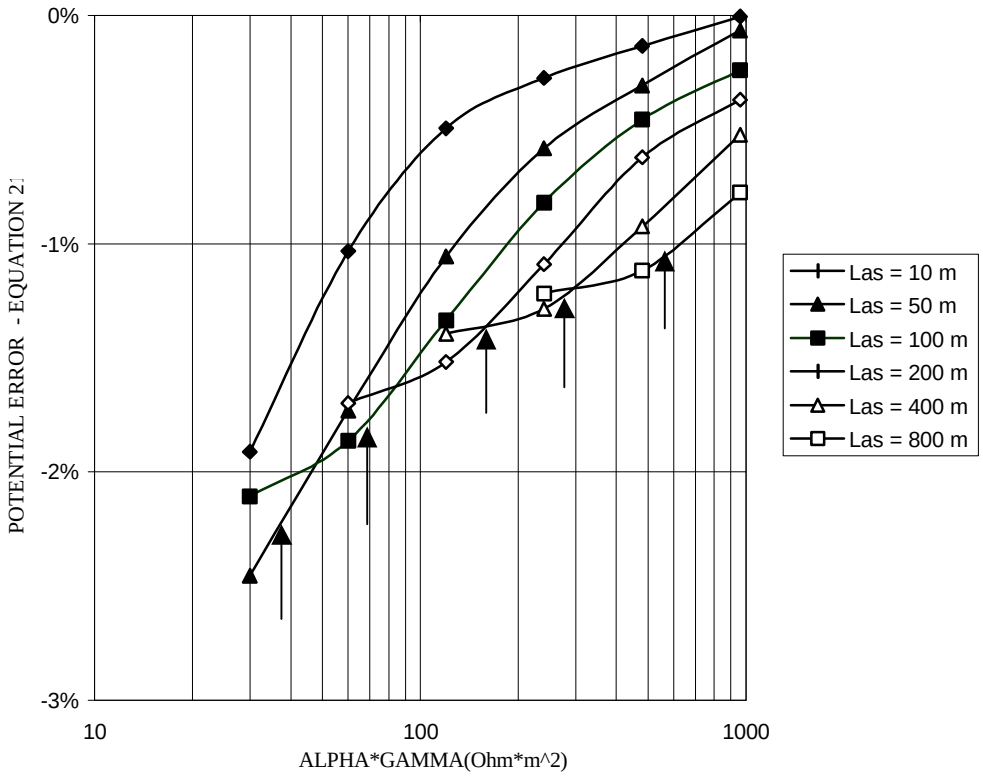

Figure 17: Error in polarized potential at the mid-anode position as determined from Equation 20 and referenced to the FDM solution to Equation 28 for r_e = 1.0 Ω.m.

Relatedly, Figure 18 plots anode current output error versus $a \cdot g$ for the same conditions as in Figure 17 where a negative error indicates greater current output per the FDM solution than what is projected by Equation 20. The percent error in current output at a particular $a \cdot g$ is greater than for potential (Figure 16) but is still acceptable for most engineering applications. Similarly, for the same design parameters but with a 0.15 Ω·m electrolyte, the maximum mid-spacing potential and anode current output errors are –1.5 and –5.0 percent, respectively, which are less than for the 1.0 Ω·m electrolyte. In the latter case, an additional calculation is necessary to confirm that adequate anode mass is available. Then, by resolving Equation 23 using defined values for all other parameters (C = 1700 Ah/kg and u =0.8), the minimum acceptable $a \cdot g$ for anodes to achieve a 30 yr design life (that is, to maintain $f_c \leq$-0.80 $V_{Ag/AgCl}$) was determined. The results of this calculation, along with the corresponding f_c values, as calculated iteratively using Equations 20 and 23, are listed in Table 6 and are indicated for each L_{as} in Figure 17 by an arrow (no arrow is shown for L_{as} = 10 m since the minimum $a \cdot g$ for this anode spacing is below 30 Ω·m^2). In the high $a \cdot g$ regime, the errors are relatively small (the negative error indicates greater polarization according to the FDM solution compared to Equation 23), they converge with increasing $a \cdot g$, and order in proportion to anode spacing (larger error the greater the anode spacing). The proposed design method has the advantage of providing an iterative approach whereby different parameters, including anode spacing and cathode potential, can be optimized.

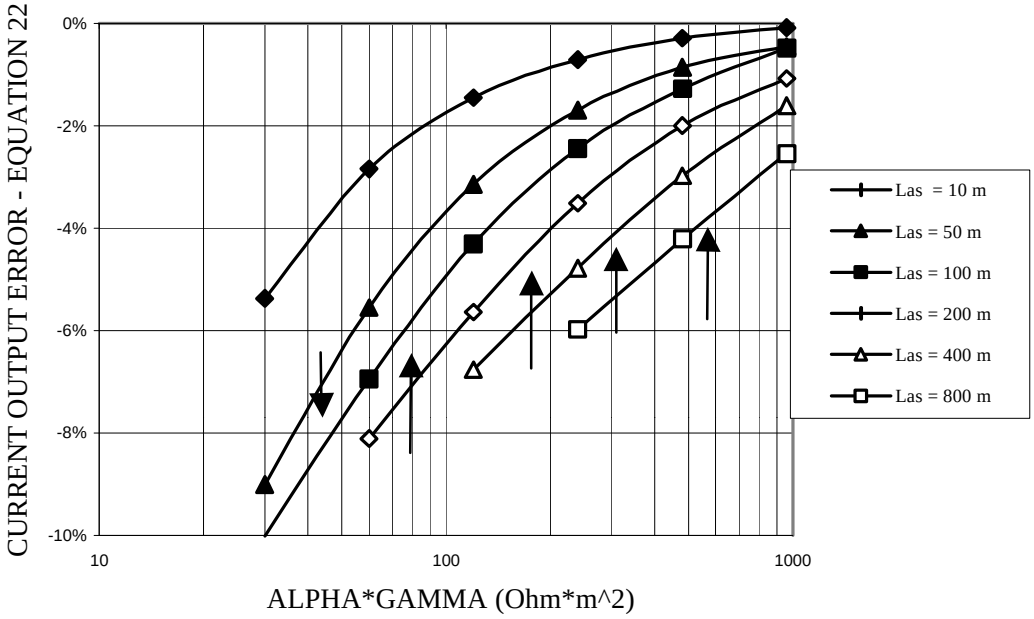

Figure 18: Error in anode current output as determined from a modified Equation 22 and referenced to the FDM solution to Equation 28 for r_e = 1.0 Ω.cm.

Table 6: Listing of the minimum allowable $\alpha \cdot g$ and the corresponding resultant cathode potential to achieve a 30 yr design life using a 133 pound (60.8 kg) anode, on a 10 in. (0.271 m) diameter pipeline in 1.0 Ω·m seawater.

ANODE SPACING, m	MINIMUM ALLOWABLE ALPHA*GAMMA, $\Omega.m^2$	RESULTANT CATHODE POTENTIAL, $V_{Ag/AgCl}$
10	7	-0.910
50	35	-0.910
100	70	-0.910
200	141	-0.910
400	282	-0.910
800	565	-0.910

TASK IV: DEFINITION AND EXAMINATION OF CRITICAL ISSUES RELATED TO PIPELINE CATHODIC PROTECTION RETROFITS

Detection of Pipeline Anode Expiration

For fixed offshore platforms, the near-expiration of standoff galvanic anodes and approaching end of the useful life of the cp system is commonly signaled by a gradual increase in potential to more positive values over one or several years. This results because of the decreased anode radius from corrosion and a corresponding increase in anode resistance which, in turn, causes I_a (Equation 1) and, hence, the magnitude of polarization to decrease. In view of this, an analysis of the potential change that might accompany expiration of a galvanic bracelet anode was performed based upon attenuation profiles projected using the FDM solutions to Equation 28. The $\acute{a} \cdot \tilde{a}$ employed was based upon $\alpha = 20\ \Omega \cdot m^2$ and assumed that g

decreased with time because of coating deterioration according to the expression (9),

$$\gamma = \frac{1}{f} = \frac{1}{0.07 + 0.004(T - 20)}. \qquad (39$$

Table 7 lists the pipe, anode, and electrolyte parameters that were employed in this evaluation. Based upon these, various exposure time increments were defined; and the anode current at the beginning of each increment and the anode mass loss for each increment were calculated. Table 8 lists the results for this. It was assumed that end of the cp service life was reached at u =0.8 (remaining anode mass 27 pounds (12.2 kg)) which occurred at year 23. The fact that this time is relatively short resulted from conservatism that is thought to be associated with the assumed g and its time dependence. Figure 19 shows the potential attenuation profiles that were calculated for the end of the different time increments. The latter plot indicates that potential of the pipeline beyond the field of the anode (z beyond about 10 m) varied over the life of the cp system by only about 20 mV and during the final year by about 10 mV. This is within the

Table 7: Pipe, anode, and electrolyte parameters employed in the cp system expiration analysis.

Pipeline Outer Radius, m	0.136
Pipeline Inner Radius, m	0.128
Anode Spacing, 2L, m	402
Equivalent Sphere radius of Anode, m	0.201
Electrolyte Resistivity, Ω.m	0.3
Pipe Resistivity, Ω.m	17×10^{-8}
Free Corrosion Pipe Potential, $V_{Ag/AgCl}$	-0.65
Anode Potential, $V_{Ag/AgCl}$	-1.05
Original Anode Radius, m	0.136
Original Anode Length, m	0.432
Anode Current Capacity, Ah/kg	1,700
Original Anode Mass, kg	60.8
Anode Utilization Factor	0.8
Alpha, Ω.m^2	20
Gamma	14.1 (1-20 years)
	13.5 (20-21 years)
	12.9 (21-22 years)
	12.3 (22-23 years)

Table 8: Calculated anode wastage parameters for different times.

Time, years	0-5	6-10	11-15	16-20	20-21	21-22	22-23
Anode Current, A	0.415	0.413	0.410	0.407	0.429	0.444	0.462
Anode Mass Loss, kg	10.6	10.6	10.6	10.4	2.2	2.3	2.2
End Anode Mass, kg	50.2	39.6	29.2	18.8	16.6	14.3	12.1
End Anode Length, m	0.415	0.390	0.365	0.338	0.333	0.330	-
End Anode Radius, m	0.181	0.175	0.167	0.158	0.156	0.154	-

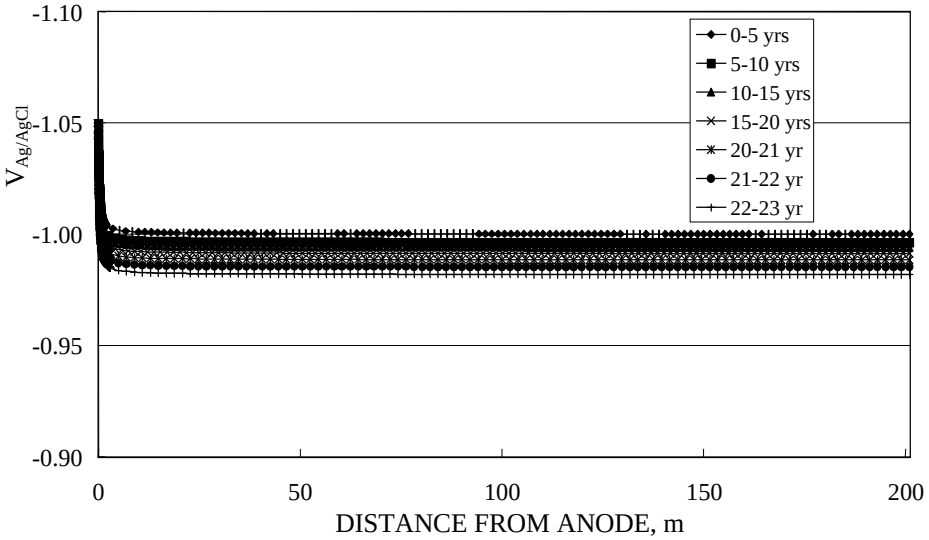

Figure 19: Potential attenuation profiles for a pipeline protected by galvanic bracelet anodes as a function of age.

range of normal variability and of measurement accuracy, and so it is concluded that insufficient pipe depolarization accompanies anode wastage to disclose pending loss of protection. Lack of potential sensitivity upon anode wastage resulted because the difference between the initial and final anode radii is relatively small for the bracelet type of design.

Principle Design Parameters for Pipeline CP Retrofit

Although not necessarily recommended, one retrofit cp alternative in the case of platforms is one-to-one replacement of the original stand-off anodes. Such an option is impractical for pipelines with galvanic bracelets, however; and so other options must be considered. For these, the cost of ship and diver/ROV time associated with anode installations along the pipeline are controlling and dictate that the guiding principle for retrofit cp design should be maximization of the spacing between anodes so that as few installations as possible are involved. An exception may arise, however, if geographical features of the bottom terrain favor a lesser anode spacing.

The parameter of greatest significance for any marine cp design, including that for pipelines, is the current density demand of the structure. Design values for new pipelines based upon bare surface area were noted earlier as ranging from 60 to 220 mA/m^2 depending upon pipe depth, temperature, and sea water versus mud exposure (10). For Gulf of Mexico applications, a design value of about 20 mA/m^2 (2 mA/ft^2) based upon the coated surface area has historically been employed. In general, anode or anode array size varies directly and spacing indirectly with magnitude of the design current density. Consequently, the economic benefits to defining a design current density with minimal uncertainty and, hence, without an unnecessarily high factor of safety (over-design) can be substantial. This is particularly

true for retrofits, although not necessarily for new construction, since in the latter case the material and installation costs of bracelet anodes are a small fraction of the total project expense. For retrofits, however, it is the number of anodes or anode array installations that is likely to be controlling, as noted above.

Pipeline Current Density Demand

As noted above, the $\acute{a} \cdot \tilde{a}$ term in Equations 20, 23, and 28 is, in effect, the pipe current density demand; and two options have been identified for determining this parameter for existing pipelines based upon survey data. Consider, for example, Equation 20 as,

$$L_{as} = \frac{(f_c - f_a)}{f_{corr} - f_c} \cdot \frac{a \cdot g}{2p \cdot r_p \cdot R_a}. \qquad (20$$

An inherent assumption built into this expression is that the pipeline is polarized such that f_c is spatially invariant (the fact that potential attenuates in the immediate vicinity of anodes is neglected as explained earlier, see Figure 16). This condition should be met for all situations where bracelets continue to provide either full or partial protection and metallic path resistance is negligible. The latter condition (negligible metallic path resistance) should be met by original designs involving gacp because bracelet anode spacing is relatively small. It may not be met, however, for pipelines that have already been cp retrofitted and for which L_{as} is relatively large. Since L_{as} and r_p are known from the original design or can be measured, f_{corr} can be estimated (a value of –0.65 $V_{Ag/AgCl}$ is commonly assumed), f_c and f_a should be available from survey data (it may be necessary to estimate f_a because of *IR* drops that may be included in measured anode potentials), and R_a can be estimated from anode dimensions or, if necessary, a value assumed since, as noted above R_a does not vary greatly as the anode wastes (see Figure 19), the parameter $\acute{a} \cdot \tilde{a}$ can be calculated directly from Equation 20 such that the current demand is known.

Example Calculation of Pipe Current Density Demand

An example application of the above method was performed based upon the pipe and electrolyte parameters listed in Table 9. Using these, a potential attenuation plot was generated using Equation 28 for the purpose of simulating survey f_c versus *z* data. Values for f_c, f_a, f_{corr}, L_{as}, r_p, and R_a (Table 9) were then substituted into Equation 20; and the corresponding values for $a \cdot g$ were calculated as an estimation of current density demand. Two values for f_c were employed, one being the far field value (f_c(FF)) at L_{as}/2 and the other an average potential (f_c(Av)) determined by numerically integrating the area under the potential-distance curve and dividing this by the half anode spacing. Table 10 shows the results of these determinations and indicates that the maximum difference between the actual and calculated current density demand was ten percent which is considered excellent agreement. Also, there is no practical difference between the current density demand calculated based upon f_c(FF) compared to f_c(Av), indicating that the

Table 9: Pipe and electrolyte parameters employed for the example $a \cdot g$ determinations.

	Example Number			
	1	2	3	4
Pipe Outer Radius, m	0.135			
Pipe Inner Radius, m	0.128			
Electrolyte Resistivity, $\Omega.m^2$	0.30			
Pipe Resistivity, $\Omega.m^2$	$17x10^{-8}$			
Pipe Corrosion Potential, $V_{Ag/AgCl}$	-0.650			
Anode Length, m	0.432	0.216		
Anode Radius, m	0.374		0.187	
Anode Potential, $V_{Ag/AgCl}$	-1.05			
Anode Spacing, m	400			200
Anode Resistance, Ω	0.0799	0.1002	0.1707	
Actual Alpha.Gamma (Eqn. 28), $\Omega.m^2$	200	100	200	100

Table 10: Results of pipe current density demand determinations based upon the Slope Parameter method.

Calculated Parameter	Case Number							
	1		2		3		4	
	f_c (FF)	f_c (Av)	f_c (FF)	f_c (Av)	f_c (FF)	f_c (Av)	f_c (FF)	f_c (Av)
Assumed Pipe Potential, $V_{(Ag/AgCl)}$	-1.000	-1.001	-0.993	-0.994	-0.908	-0.91	-0.966	-0.967
Calculated Alpha.Gamma, $\Omega.m^2$	190	195	205	210	105	107	108	110
Difference Compared to Actual Alpha.Gamma (Table 9), percent	-5	-2.5	2.5	5	5	7	8	10
Current Output per Anode Based on Actual ag (Eqn. 28), A	0.595		0.583		0.883		0.538	
Current Output per Anode Based on Calculated ag, A	0.625	0.618	0.569	0.557	0.832	0.822	0.495	0.486
Difference Compared to Actual Alpha.Gamma (Table 9), percent	5	4	-2	-4	-6	-7	-8	-10

pipe potential gradient in the vicinity of the anode exerted little influence. The anode current outputs as determined by 1) the FDM solution to Equation 28 (these were assumed to be the actual or correct values) and 2) the Slope Parameter method using the calculated $a \cdot g$ values are also listed. The difference between these tracks that of the current demand results, as should be expected.

An alternative approach to estimating current density demand involves application of a rearranged form of Equation 28. Unlike the case above (Equation 20), Equation 28 applies to situations where potential continues to attenuate beyond the field of the anode. Thus, by rearranging Equation 28,

$$ag = \frac{-\frac{\partial E(z)}{\partial z} \cdot r_e r_p \cdot (\frac{1}{r_a} - \frac{1}{z}) - E(z) \cdot [\frac{2 r_e r_p}{z^2} - R_m \cdot 2p \cdot r_p] + \frac{2 r_e r_p}{z^3} \int_z^L E(t) dt}{\frac{\partial^2 E(z)}{\partial z^2}}, \qquad (40$$

and then $á \cdot ã$ can be solved for based upon defining values for *E(z)* and the first and second derivatives thereof (Equations 29 and 30, respectively) at selected *z* from survey data that indicate the potential profile. As an evaluation of this approach, values for *E(z)*, *E'(z)*, and *E"(z)* for the attenuation profile that resulted from cp for the same pipe and electrolyte parameters as in Table 4 but with $á \cdot ã$ = 200 Ω.m^2 and L_{as} = 200 m were measured at selected values for *z*. These *z's* are necessarily near the anode because the potential profile becomes flat beyond this and relatively large errors in the calculated E' and *E"* are likely here. Figure 20 shows the attenuation profile that was determined based upon Equation 28, and Table 11 lists the results of the hind-sight $á \cdot ã$ calculation for five different *z* values using Equation 40. This shows that the calculated values differ from the actual by from –25 to +61 percent. Such error is relatively large and presumably resulted because *E(z)* varies sharply with *z* near the anode and minimally beyond about ten m. This promotes error in one or more of the input potential parameters. The results do indicate, however, that it should be possible to estimate $á \cdot ã$ within a factor of two. Note, however, that the error was minimal (6.0 and 10.5 percent) at *z* = 4 and 5 m, respectively. With further study, it may be possible to identify an ideal *z* at which $á \cdot ã$ should be estimated using this method.

Of the two methods (Slope Parameter (Equation 20) or FDM (Equation 40)), the former provided the better accuracy; and so it is the recommended approach. If, however, attenuation persists beyond the field of the anode, as should occur where pipe resistance is a factor, then the approach based upon Equation 40 is

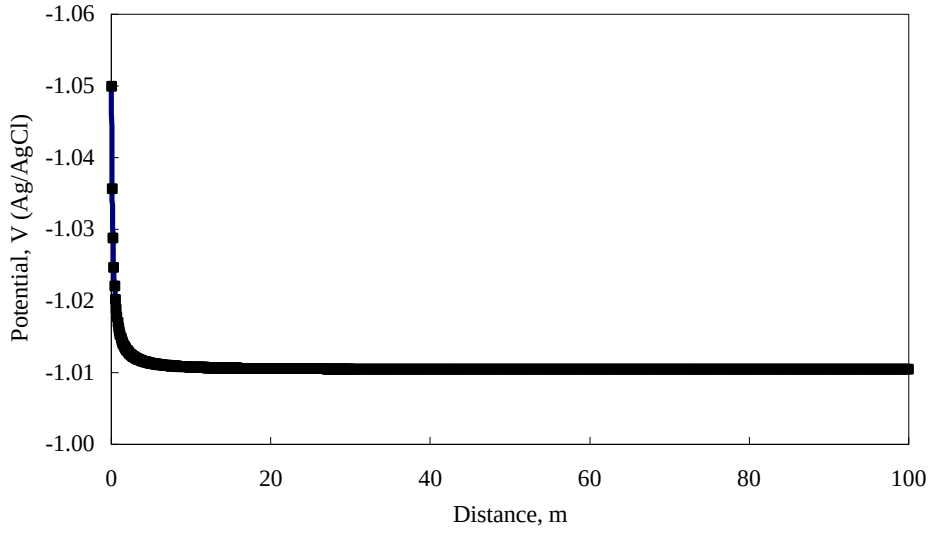

Figure 20: Calculated attenuation profile.

Table 11: Calculated parameters for the current density demand protocol.

z, m	*z* Increment	Potential, $V_{Ag/AgCl}$	*E(z)*, V	*E'(z)*	*E''(z)*	*ag* Calculated	Difference, %
0.9	i-1	-1.01630					
1.0	i	-1.01574	-0.3657	5.143E-03	-8.950E-03	322	61
1.1	i+1	-1.01527					
2.9	i-1	-1.01213					
3.0	i	-1.01207	-0.3621	6.455E-04	-4.300E-04	239	19.5
3.1	i+1	-1.01200					
3.9	i-1	-1.01162					
4.0	i	-1.01159	-0.3616	3.600E-04	-2.000E-04	212	6
4.1	i+1	-1.01155					
4.9	i-1	-1.01132					
5.0	i	-1.01130	-0.3613	2.430E-04	-9.600E-05	221	10.5
5.1	i+1	-1.01128					
6.9	i-1	-1.01100					
7.0	i	-1.01099	-0.361	1.075E-04	-5.000E-05	150	-25
7.1	i+1	-1.01098					

the only alternative.

The above methods do not account for presence of residuals from the original anodes or exposed bare steel portions of the bracelets. In effect, these serve as bare areas on the pipeline that will tend to drain the cp current. Also, potential of any residual anodes, f_a(residual), will probably be more positive than for the retrofit anodes, f_a(retrofit), in which case they will draw current also. Visual observations and potential survey data should be helpful it defining this situation. If bare steel only is present, then the coating bare area term, *g*, should be adjusted to reflect this and an overall current density demand calculated. For the case where residuals from the original anodes are present, current demand should be less than for the steel-only situation since the potential difference between these anodes and the new ones should be less than when residuals are not present. In cases where the original anodes have corroded to a point where both these and bare steel are present, a common mixed potential that is intermediate to both that of freely corroding steel and of the residual anodes should be employed. On this basis, it can be reasoned that the additional current that must be provided by the retrofit cp system because of an anode residual, I_b, is,

$$I_b = \left(i_c \cdot A_r\right) \cdot \left(\frac{f_a(\text{retrofit}) - f_a(\text{residual})}{f_a(\text{retrofit})} \right), \qquad (41$$

where i_c is the residual current density demand of the bare metal (steel or aluminum or a combination of the two), and A_r is surface area of a residual. It can be assumed that i_c for the residual aluminum is the same as for steel. This approach assumes, however, that voltage drop associated with the bare areas is negligible,

which may not be the case. Boundary Element Modeling can provide insight into any limitations that presence of bare metal might impose upon the proposed approach.

Anode/Anode Array Design

As noted above, the effect of 1) pipe current density demand, 2) anode/anode array design, and 3) anode/anode array spacing is, in general, interrelated. Stated differently, it is current density demand and anode/anode array resistance combined that determine the distance from an anode to which a pipeline is protected. Consequently, optimization of the anode/anode array design is a key aspect in affecting an efficient, effective retrofit cp system. If maximization of retrofit anode spacing is a design criterion, then this translates to achieving as low a value for R_a as is practical. Equation 38 indicates that anode resistance decreases in proportion to electrolyte resistivity and varies inversely with anode surface area. This statement applies generally to all geometries and not just bracelets (17). Thus, influence of the former parameter (resistivity) is such that anode arrays should be positioned above the mud bottom if at all possible, since resistivity of mud is invariably greater than for sea water per se; and the support structure (sled, for example) should be designed such that they remain so. In light of the surface area dependence of anode resistance, the incentive for achieving low resistance is generally addressed by employing multiple anodes (an array) with a common electrical connection to the pipeline rather than a single large anode (see Equation 5). However, Equation 5 applies in situations where anodes are spaced sufficiently far apart that interaction effects are negligible. Because it is impractical to widely separate anodes in most pipeline retrofit anode array designs, interactions must be taken into account. Closed-form numerical solutions for resistance of different configurations for multiple anodes are available in the literature (16-21); or, alternatively, resistance can be calculated using BEM. Because the latter method can be expensive and requires special training, numerical solutions are preferred for engineering practice. However, existing resistance equations do not necessarily address likely configurations for pipeline retrofit anode arrays.

The case of non-interacting anodes (or at least anodes that are assumed not to interact) is relevant to pipelines that receive protection from a platform to which they connect. In this regard, the equivalent resistance spherical anode concept can be extended to this case by combining Equation 5 with the expression for resistance of a spherical conductor to remote earth,

$$r_a = \frac{r_e}{4pR_t}, \qquad (42$$

to yield

$$r_a = \frac{r_e \cdot N}{4pR_a}. \qquad (43$$

Figure 21 plots this radius versus N and shows that r_a exceeds 50 m for a structure with 200 725 pound (330 kg) anodes. Application of Equation 42, upon rearranging, to a 50 m diameter spherical anode indicates its resistance in 0.15 Ω.m sea water to be 0.00048 Ω, which is approximately two orders of magnitude less than for a single anode. Analyses have not yet been performed to determine the accuracy with which the spherical anode concept can be applied in such situations and the extent to which a pipeline can be protected by a platform.

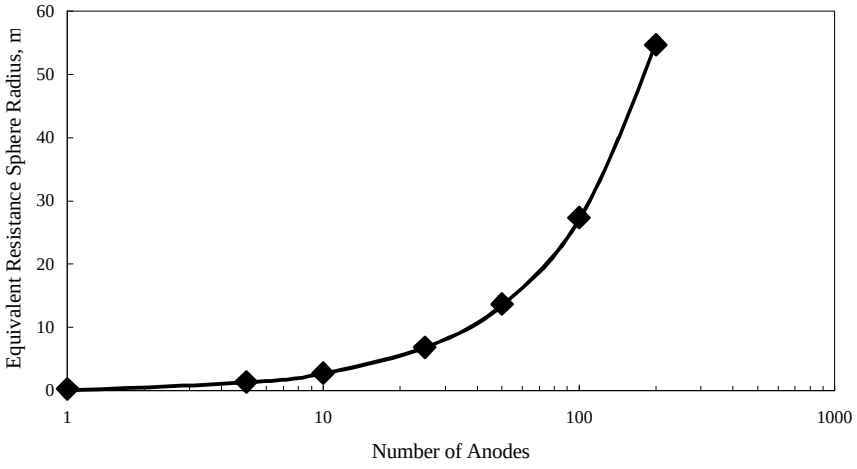

Figure 21: Plot of the radius of a single, equivalent resistance spherical anode versus the number of actual anodes for the case where anodes do not interact.

Resistance determinations for situations where anodes do interact, as is likely to be the case for retrofit anode arrays, can be made based upon the analysis proposed by Pierson and Hartt (34) for well conductors, considering that n equal size anodes of length, l, and radius, r, where $l >> r$ and $N/4$ is a whole number, are arranged in a periodic square array. Here, the equivalent resistance of each group of four contiguous anodes, $R(4)$, is determined using Sunde's equation for n parallel, deeply submerged, identical electrodes spaced equally about the perimeter of a circle as,

$$R(N) = \frac{1}{N}\left[R1(r) + \sum_{m=1}^{N-1} R1\left(D\sin\left(mp / N\right)\right)\right], \qquad (44$$

where D is diameter of the circle, and $R1$ and $R1(Dsin[mp/m])$ are generated from Sunde's equation (17) for resistance of a single, deeply submerged cylindrical electrode by the average potential method as,

$$R_1 = \left[\frac{r_e}{2pl}\right] \cdot \left[ln \frac{l\left(1+\sqrt{1+(r/l)^2}\right)}{r} \right] + \frac{r}{l} - \sqrt{1+(r/l)^2} \ . \qquad (45$$

Thus, for four identical electrodes equally spaced about a circle, as shown in Figure 22, Equation 40 becomes,

$$R_N = \frac{1}{4}\left[R1(r) + 2\left[R1(D\,sin(p\ /\ 4)) + R1(D)\right]\right]. \qquad (46$$

Also shown is the circumference of the single, equivalent resistance electrode. For values of *n* other than four (but with *n*/4 still equaling a whole number), the process is repeated until a single electrode remains.

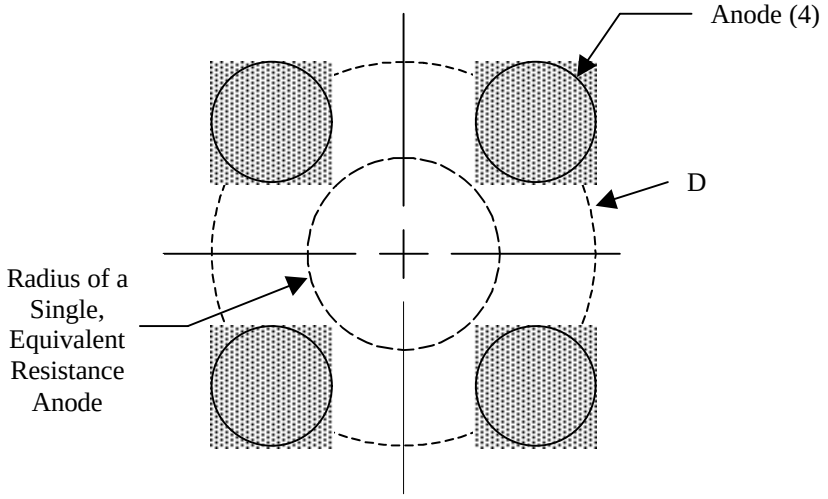

Figure 22: Schematic illustration of the equivalent resistance algorithm for a square array of four electrodes.

A more general situation, however, is that of a rectangular array for which *n*/4 is not necessarily a whole number. Here, the equivalent resistance, R_n, can be estimated by a sequential calculation, the first step of which involves Sunde's equation (17) for the equivalent resistance of a deeply submerged, linear array of identical electrodes spaced a distance *s* apart as,

$$R_N = \frac{1}{N}\left(R1(r) + \frac{2}{N}\left[(N-1)R1(s) + (N-2)R1(2s) + \cdots + R1(Ns-s)\right]\right). \qquad (47$$

and its equivalent resistance determined. Next, the equivalent resistance of each row is calculated; and each row is replaced by a single electrode, the radius of which corresponds to this equivalent resistance.

The equivalent resistance of the single resultant column is then calculated and is the equivalent resistance for the overall array.

Figure 23 illustrates the geometry for a recently designed and deployed marine pipeline retrofit anode sled that was comprised of four inclined (69^{o} to the horizontal) trapezoidal cross section anodes of equivalent radius 0.089 m (3.50 in) and length 2.44 m (8.0 ft). Thus, in order to provide horizontal stability, the electrodes in actual anode arrays are not necessarily parallel. To investigate the effect of this

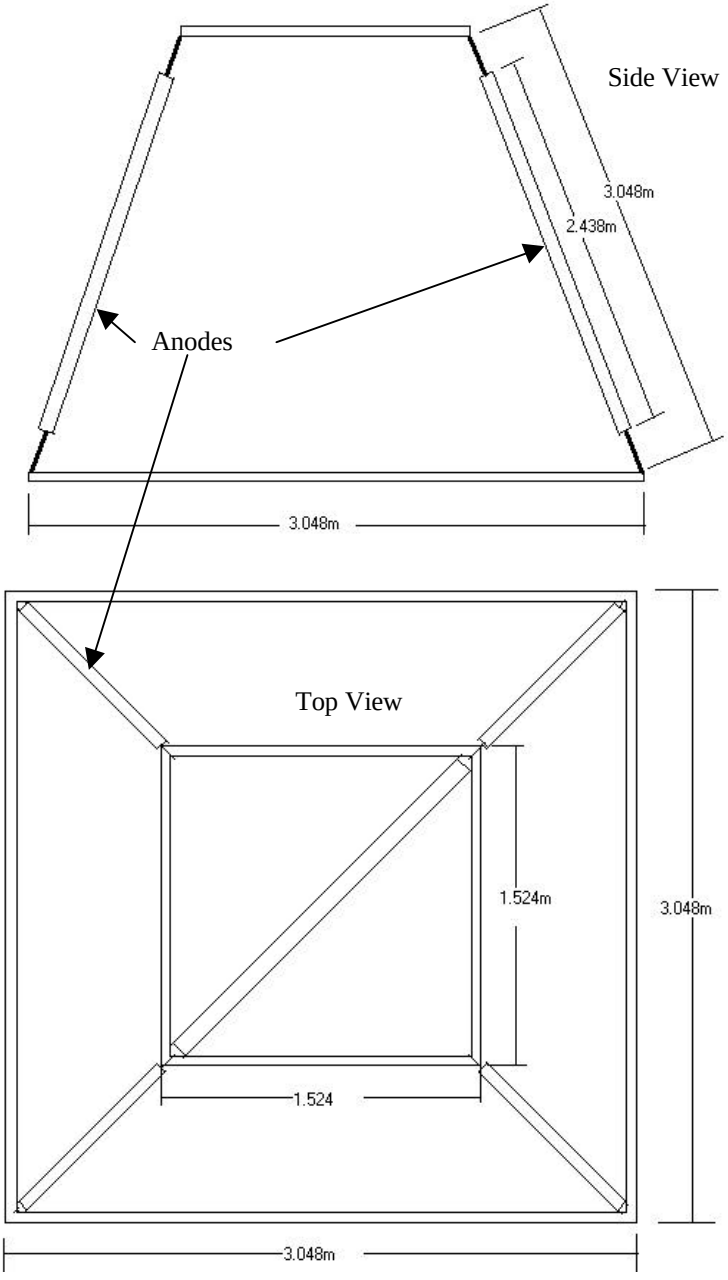

Figure 23: Schematic illustration of a four-anode pipeline retrofit array.

non-parallelism, equivalent resistance of the array was calculated using, first, Equation 43 assuming the electrodes are parallel and, second, BEM based upon the actual (inclined) configuration. In the former case, R_n = 0.0233 Ω and in the latter 0.0237 Ω, such that the difference between the two equivalent resistances is less than two percent. The corresponding equivalent spherical radius is 1.137 m.

The resistance of the array in Figure 23 decreases as either the number or size of the anodes increases (or both). For example, Table 12 lists the resistance of the same sled as above but with 725 pound (330 kg) anodes (equivalent radius 0.52 ft (0.159 m)). Also included is resistance of a 16 725 pound (330 kg) square pattern array with anodes spaced at two m (center-to-center). This indicates that, in addition to the Equation 42 and BEM results being in good mutual agreement, the resistance decrease associated with increased anode sizing is relatively modest but that the 4x4 array resistance is about one-half that of the 2x2.

Table 12: Resistance of different anode arrays.

Array Type	Resistance (BEM), Ohms	Resistance (Eqn. 41), Ohms
2x2	0.021	0.021
4x4	0.0112	0.0119

Maximized Anode/Anode Array Spacing

Either of two approaches can be taken to optimize anode/anode array spacing. The first of these is relevant when the pipeline terminates at and receives cathodic protection from a relatively large structure. Equation 5 indicates that anode resistance for such situations is very low provided N is sufficiently large, in which case the Uhlig/Morgan equation (Equation 14) applies. This expression can also be used in non-zero anode resistance situations provided the potential at the drainage (electrical connection) point, E_a in Equation 14 and Figure 1, is known. If the pipeline is at "remote earth" relative to the platform, then a closed form numerical solution can be used to calculate anode resistance and voltage drop. In this case, pipe potential at the drainage point, E_a, equals the potential at the anode surface minus this voltage drop. Alternatively, BEM can by employed, irrespective of whether or not the anode/anode array is positioned remotely from the pipeline.

Accuracy of the above type of anode/anode array resistance modeling may be limited, however, if a portion of the pipe is positioned within the radius of the equivalent resistance anode. Alternatively, the pipeline may be positioned within the potential field of one or more anodes of the array despite its being remote with respect to the field of the equivalent resistance anode.

A second approach was developed from the first-principles based attenuation equation (Equation 28). However, because this expression pertains to equally spaced superimposed anodes, as is typical in new construction but impractical for retrofits, modification of the model upon which this equation is based becomes necessary. Figure 24 shows a schematic illustration of the proposed offset anode model. This defines the center-to-center offset distance from the pipe of a spherical anode as *OF* and the distance of the anode from a point z_x on the pipe as d_x, where,

$$d = \sqrt{OF^2 + z^2} \ . \qquad (48$$

Development of a governing equation for this situation using the same approach that yielded Equation 28 resulted in the expression,

$$\frac{\partial^2 E(z)}{\partial z^2} + \frac{\partial E(z)}{\partial z} \cdot H\left(\frac{1}{r_a} - \frac{1}{d}\right) + E(z) \cdot \left[\frac{2zH}{d^3} + B\right] = -QH \int_z^L E(t)dt \ , \qquad (49$$

where

$$Q = \left(\frac{1}{d^3} - \frac{3z^2}{d^5}\right). \qquad (50$$

Using an iterative, explicit finite difference scheme, Equation 49, can be solved as:

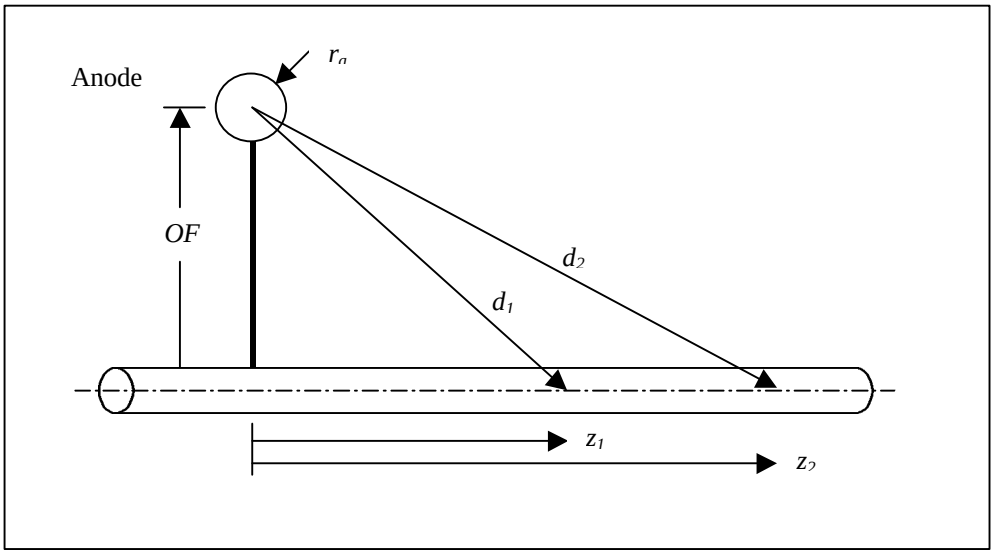

Figure 24: Model for a pipeline protected by an offset anode.

$$E_i^{m+1} = \frac{\frac{-QHdz}{2}\left(\sum_{j=1}^{N-1} 2E_{i+j}^m + E_N^m\right) + \frac{E_{i-1}^{m+1}}{dz} H\left(\frac{1}{r_a} - \frac{1}{d_i}\right) - \frac{E_{i-1}^{m+1}}{dz^2} - \frac{E_{i+1}^m}{dz^2}}{\frac{-2}{dz^2} + \frac{H}{dz}\left(\frac{1}{r_a} - \frac{1}{d_i}\right) + \left(\frac{2z_i H}{d_i^3} + B\right) + \frac{QHdz}{2}}. \quad (51$$

Equation 28 assumes the potential of the pipe element closest to the anode to be the same as for the anode. However, in the offset case, these potentials are different. Defining pipe potential at the drainage point was accomplished by, first, calculating the anode current output for the case where this electrode is superimposed upon the pipe (Equation 28) using a FORTRAN/FDM program and, second, calculating potential drop in the electrolyte from the expression,

$$Df_{r_a \to OF} = \frac{r_e I}{4p}\left[\frac{1}{r_a} - \frac{1}{OF}\right]. \quad (52$$

The pipe potential at $z = 0$ for the offset anode configuration can then estimated as,

$$f_c(z=0) = f_a - Df_{r_a \to OF}. \quad (53$$

This value is inputted to an iterative FORTRAN/FDM program and Equation 51 solved. The model was tested using the same parameters as for the earlier examples except with r_a = 0.170 m, r_e = 0.15 and 1.0 Ω.m, $á \cdot ã$ values of 100 and 1,000 Ω.m^2, L_{as} = 200, 500, 750, 1,000, and 2,000 m, and OF = 1, 5, and 10 m. The example is not realistic with regard to a retrofit situation, however, because of the small anode size. Voltage drop through the anode connection cable was assumed to be negligible.

Figures 25-27 show attenuation profiles for each of the three offset distances, r_e = 0.15, $á \cdot ã$ = 100 Ω.m^2, and anode spacings of 200, 500, 750, 1,000, and 2,000 m in comparison to results from a companion BEM analysis, where the latter employed a cylindrical anode of the same equivalent resistance as the FDM one. This water resistivity (r_e = 0.15 Ω.m) is considered to approach the lower limit of what is likely to be encountered in practice. The results indicate, first, that the BEM projects greater cathodic polarization than does the FDM solution to Equation 51 with magnitude of the difference increasing in proportion to anode spacing. This reflects, at least in part, the fact that the BEM analysis neglects metallic path resistance as discussed above. Second, potential at z = 0 is progressively more positive the greater the offset distance. Note, however, that the far field potential is virtually independent of the offset. Also, while these offset anodes provide protection at a spacing of 2,000 m and probably slightly beyond, the protection distance afforded by superimposed bracelets is less (see Figure 10). This difference presumably occurred because with the offset less current was delivered to the pipe in the immediate vicinity of the anode, and so more

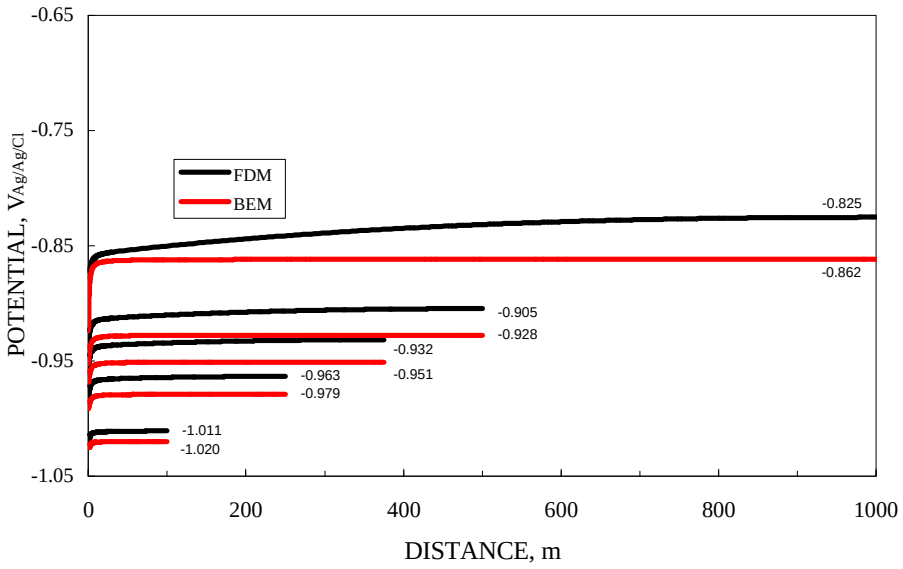

Figure 25: Attenuation plots for a 0.271 m (nominal 10 in) diameter pipeline with r_e = 0.15 Ω.m, $\acute{a} \cdot \tilde{a}$ = 100 Ω.m^2, and a 0.340 m diameter spherical anode offset at one m.

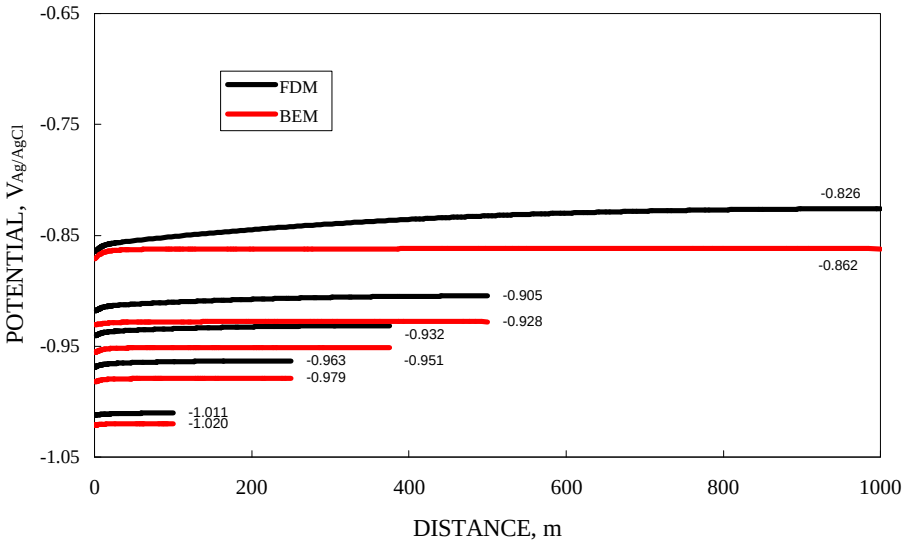

Figure 26: Attenuation plots for a 0.271 m (nominal 10 in) diameter pipeline with r_e = 0.15 Ω.m, $\acute{a} \cdot \tilde{a}$ = 100 Ω.m^2, and a 0.340 m diameter spherical anode offset at five m.

current was available at distant locations.

Correspondingly, Figures 28-30 show companion plots to the ones in Figures 25-27 but for $\acute{a} \cdot \tilde{a}$ = 1,000 Ω.m^2. The trends in the two sets of plots are similar except that 1) attenuation is less in the immediate vicinity of the anode, 2) protection of the pipe is affected at a more negative potential, and 3)

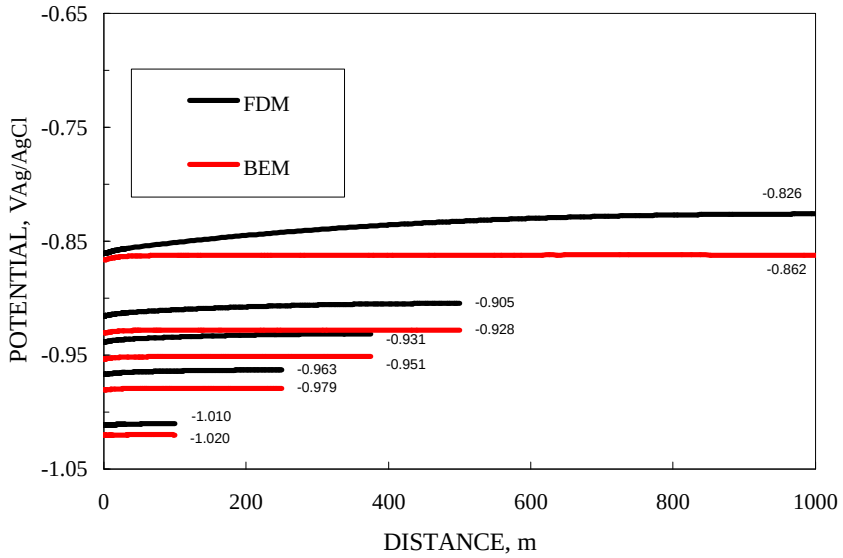

Figure 27: Attenuation plots for a 0.271 m (nominal 10 in) diameter pipeline with r_e = 0.15 Ω.m, $á \cdot \tilde{a}$ = 100 Ω.m^2, and a 0.340 m diameter spherical anode offset at ten m.

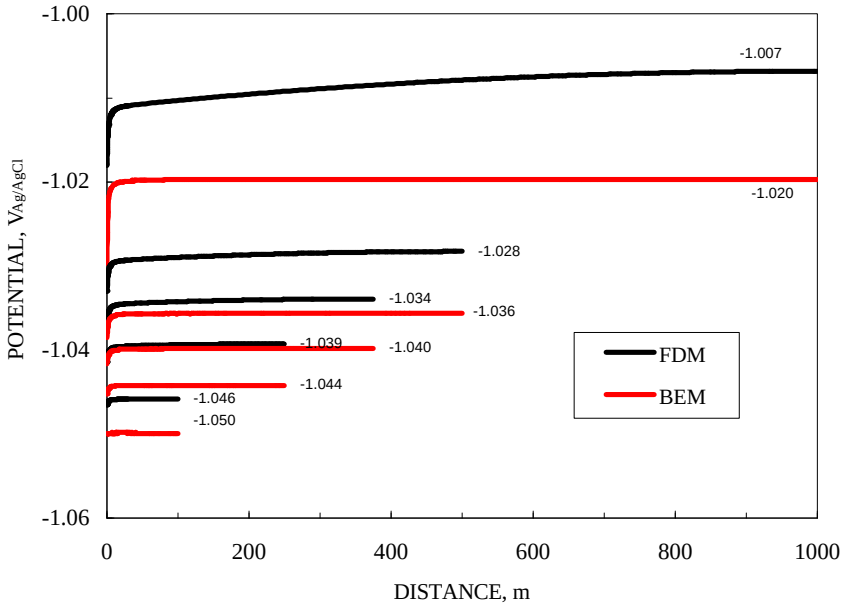

Figure 28: Attenuation plots for a 0.271 m (nominal 10 in) diameter pipeline with r_e = 0.15 Ω.m, $á \cdot \tilde{a}$ = 1,000 Ω.m^2, and a 0.340 m diameter spherical anode offset at one m.

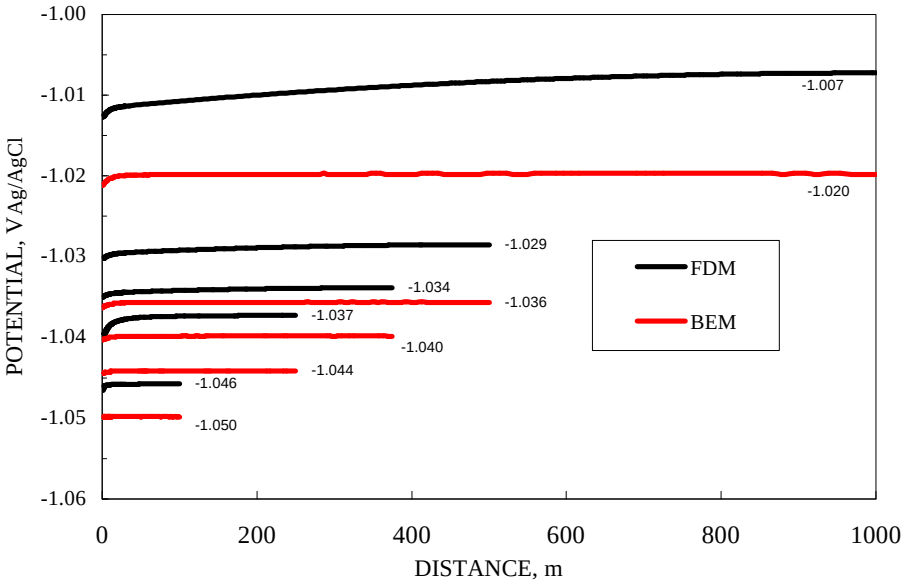

Figure 29: Attenuation plots for a 0.271 m (nominal 10 in) diameter pipeline with r_e = 0.15 Ω.m, $\acute{a} \cdot \tilde{a}$ = 1,000 Ω.m^2, and a 0.340 m diameter spherical anode offset at five m.

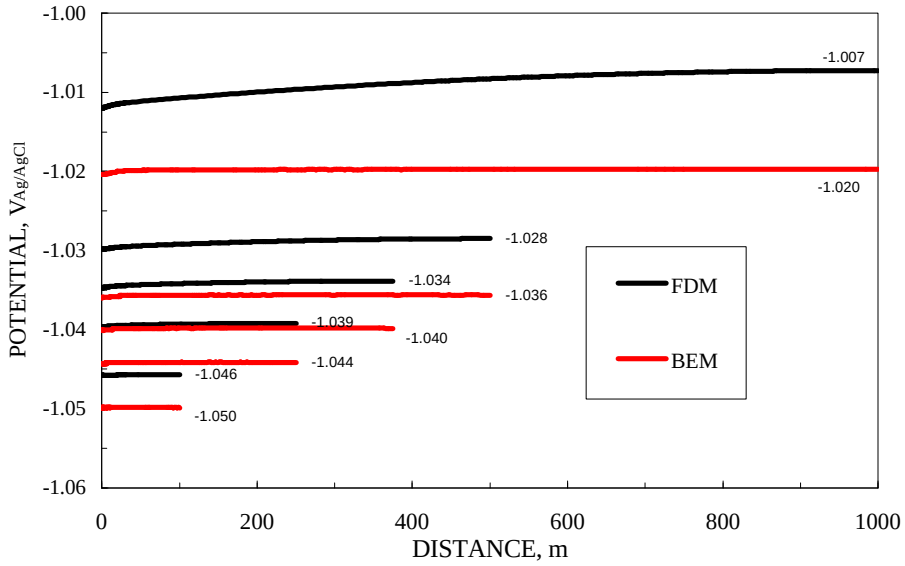

Figure 30: Attenuation plots for a 0.271 m (nominal 10 in) diameter pipeline with r_e = 0.15 Ω.m, $\acute{a} \cdot \tilde{a}$ = 1,000 Ω.m^2, and a 0.340 m diameter spherical anode offset at ten m.

protection can be realized with greater anode spacings compared to the $\acute{a} \cdot \tilde{a}$ = 100 Ω.m^2 case (note the difference in the scale of the potential axis for the two sets of plots). Consequently, these calculations were repeated using the equivalent radius for the anode array shown in Figure 23 (1.137 m). Figures 31-34 show the results of this for different combinations $\acute{a} \cdot \tilde{a}$ (100 and 1,000 Ω.m^2) and r_e (0.15 and 1.0 Ω.m) with an

offset distance of ten m in all cases. Here, the plots extend to larger anode separations in order to provide an indication of possible protection distances. BEM analyses are not included in the large anode spacing cases because of the error associated with these as explained above.

While Figures 25-30 confirm utility of the offset model and provide a comparison to the

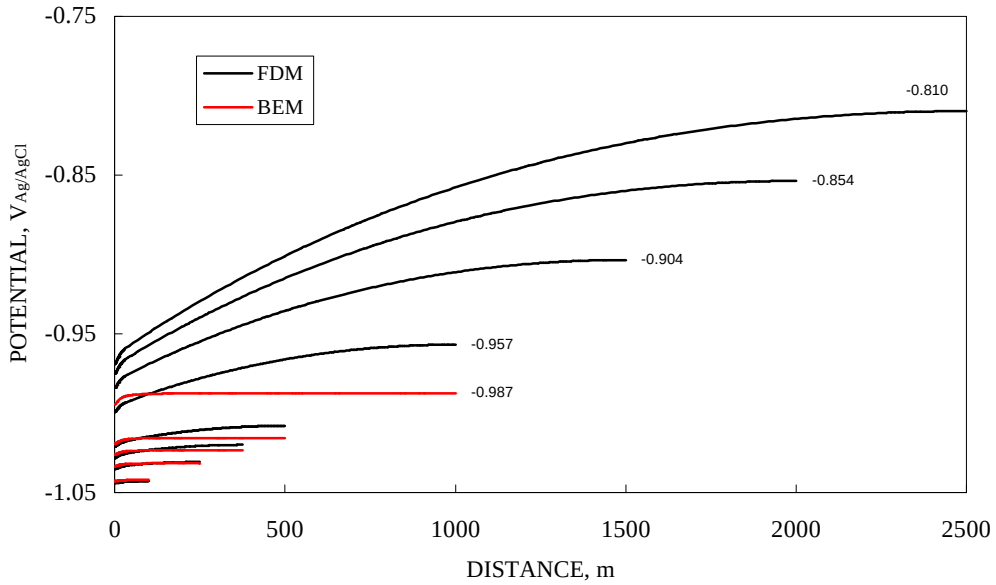

Figure 31: Attenuation plots for a 0.271 m (nominal 10 in) diameter pipeline with r_e = 0.15 Ω.m, $\acute{a} \cdot \tilde{a}$ = 100 Ω.m^2, and a 2.274 m diameter spherical anode offset at 10 m.

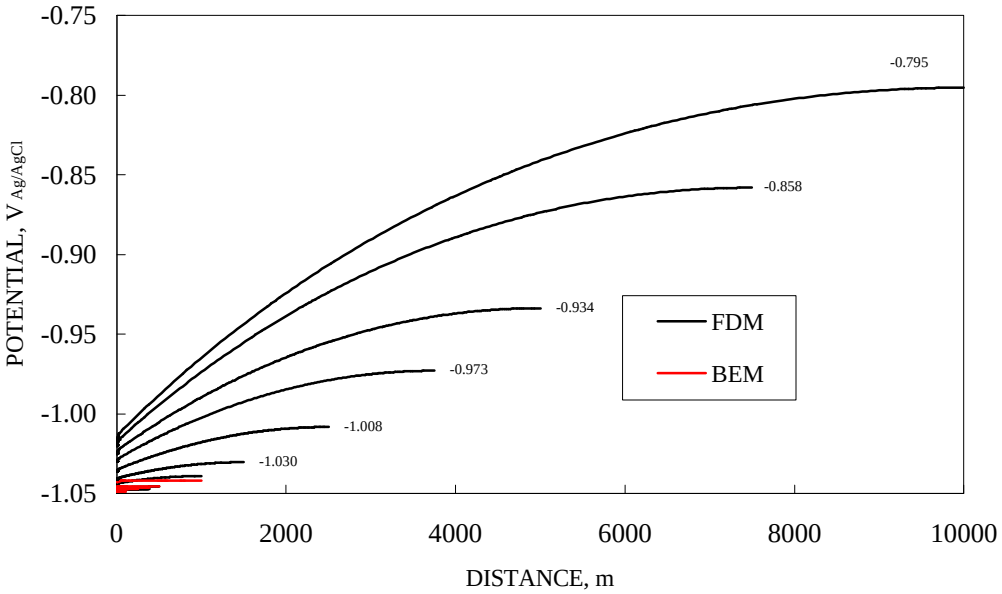

Figure 32: Attenuation plots for a 0.271 m (nominal 10 in) diameter pipeline with r = 0.15 Ω.m, $\alpha \cdot \gamma$ = 1,000 Ω.m^2, and a 2.274 m diameter spherical anode offset at 10 m.

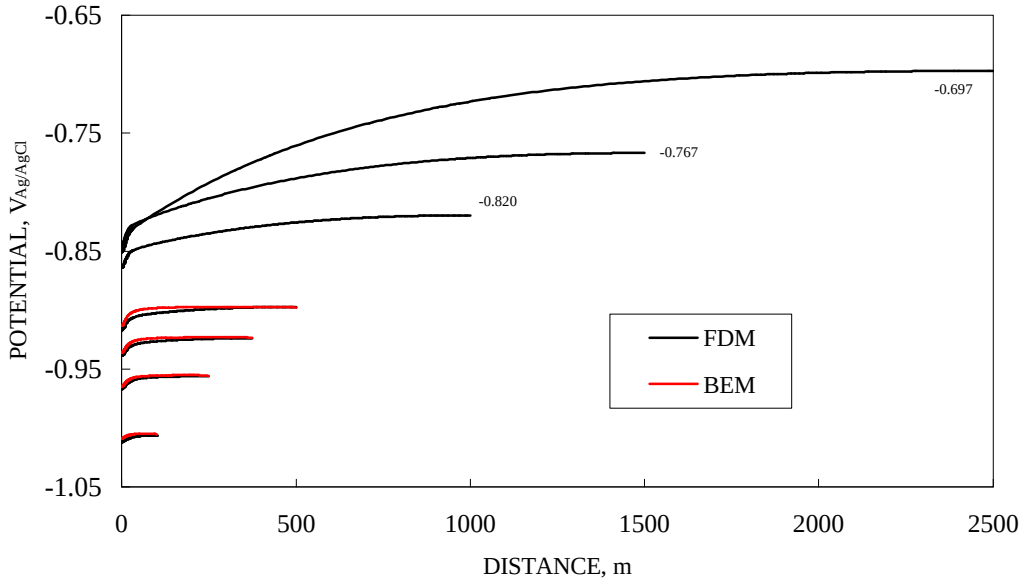

Figure 33: Attenuation plots for a 0.271 m (nominal 10 in) diameter pipeline with r = 1.0 Ω.m, $\alpha \cdot \gamma$ = 100 Ω.m^2, and a 2.274 m diameter spherical anode offset at 10 m.

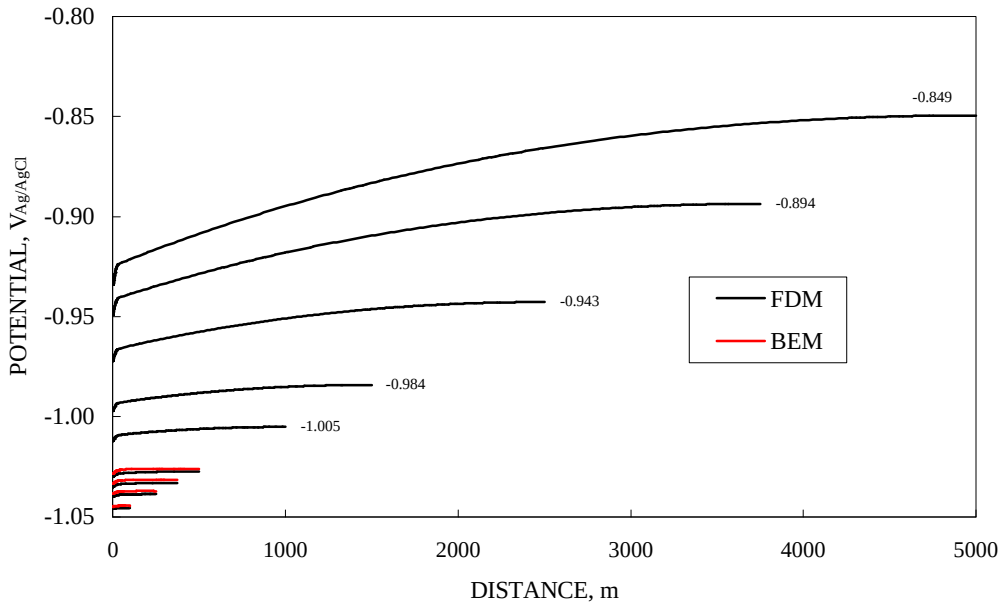

Figure 34: Attenuation plots for a 0.271 m (nominal 10 in) diameter pipeline with r = 1.0 Ω.m, $\alpha \cdot \gamma$ = 1,000 Ω.m^2, and a 2.274 m diameter spherical anode offset at 10 m.

superimposed anode case (Figures 7, 10, and 11), the physical situation is probably not relevant to a cp retrofit because of the small anode size that was involved (spherical anode with radius 0.170 m). Consequently, these calculations were repeated using the equivalent radius for the anode array shown in Figure 23 (1.137 m). Figures 31-34 show the results of this for different combinations $\acute{a} \cdot \tilde{a}$ (100 and 1,000

$\Omega.m^2$) and r_e (0.15 and 1.0 Ω.m) with an offset distance of ten m in all cases. Here, the plots extend to larger anode separations in order to provide an indication of possible protection distances. BEM analyses are not included in the large anode spacing cases because of the error associated with these as explained above.

In order to better quantify the maximum appropriate anode array spacing and the distance to which protection can be extended, Figure 35 shows a plot of potential at the mid-anode spacing as a function of that spacing for the conditions addressed in Figures 31-34 and where protection results ($f_c \leq$ -0.80 $V_{Ag/AgCl}$). Correspondingly, Table 13 lists the equation interrelating this maximum potential and spacing for each of the conditions investigated (Figures 31-34); and based upon these, Table 14 lists the corresponding anode array spacing that yields a mid-position potential of –0.85 $V_{Ag/AgCl}$, which corresponds to a 50 mV factor of safety.

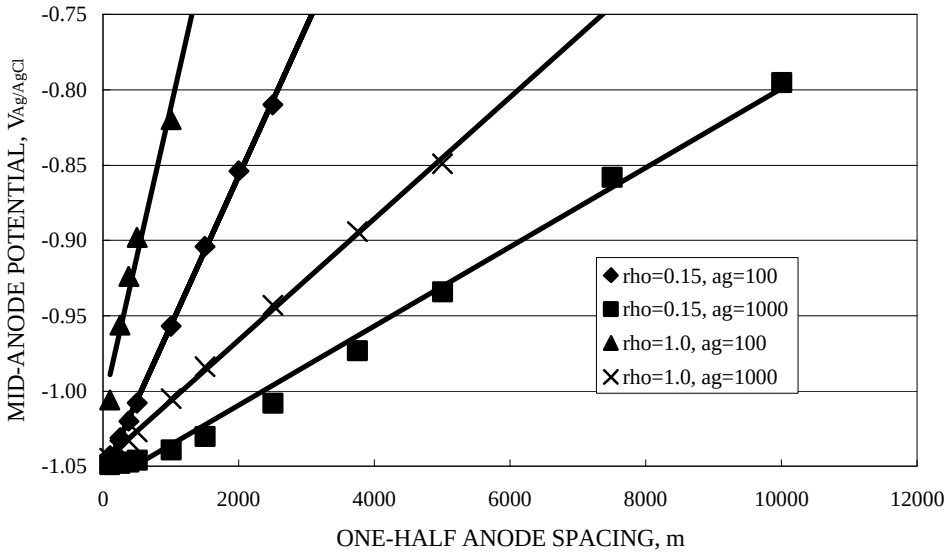

Figure 35: Mid-anode potential as a function of anode half spacing for the situations represented in Figures 31-34.

Table 13: Listing of the equation that interrelates mid-anode pipe potential and the corresponding anode spacing for the conditions investigated.

Condition	Equation
r_e=0.15, ag=100	$f_c = 10^{-4} \cdot L - 1.056$
r_e=0.15, ag=1,000	$f_c = 3 \cdot 10^{-5} \cdot L - 1.062$
r_e=1.0, ag=100	$f_c = 2 \cdot 10^{-4} \cdot L - 1.009$
r_e=1.0, ag=1,000	$f_c = 4 \cdot 10^{-5} \cdot L - 1.047$

Table 14: Listing of projected maximum anode array spacings that result in a mid-anode potential of –0.85 $V_{Ag/AgCl}$.

Water/Mud Resistivity, Ω.m	*ag*, $\Omega.m^2$	Approximate Bracelet Anode Spacing (Figs. 10 and 11), m	Approximate Retrofit Anode Array Spacing (Fig. 35), m
0.30	100	1,500	-
0.30	1,000	8,000	-
0.15	100	-	4,100
0.15	1,000	-	14,100
1.00	100	-	1,600
1.00	1,000	-	10,000

TASK V: RECOMMENDED PROTOCOL FOR RETROFIT CATHODIC PROTECTION DESIGN OF MARINE PIPELINES

Figure 36 presents a flow diagram that overviews the pipeline cp retrofit decision and design process. The critical features here are listed as follows:

1. Determination that a cp retrofit is required.

2. Determination of pipe current density demand and, hence, of the required anode current output.

3. Determination of whether anode array spacing is to be governed by factors such 1) terrain or proximity to shore or structure(s) or 2) minimization of the number of anode arrays.

4. Anode array design.

Candidate protocols and methods for addressing each of these are presented under Task IV above.

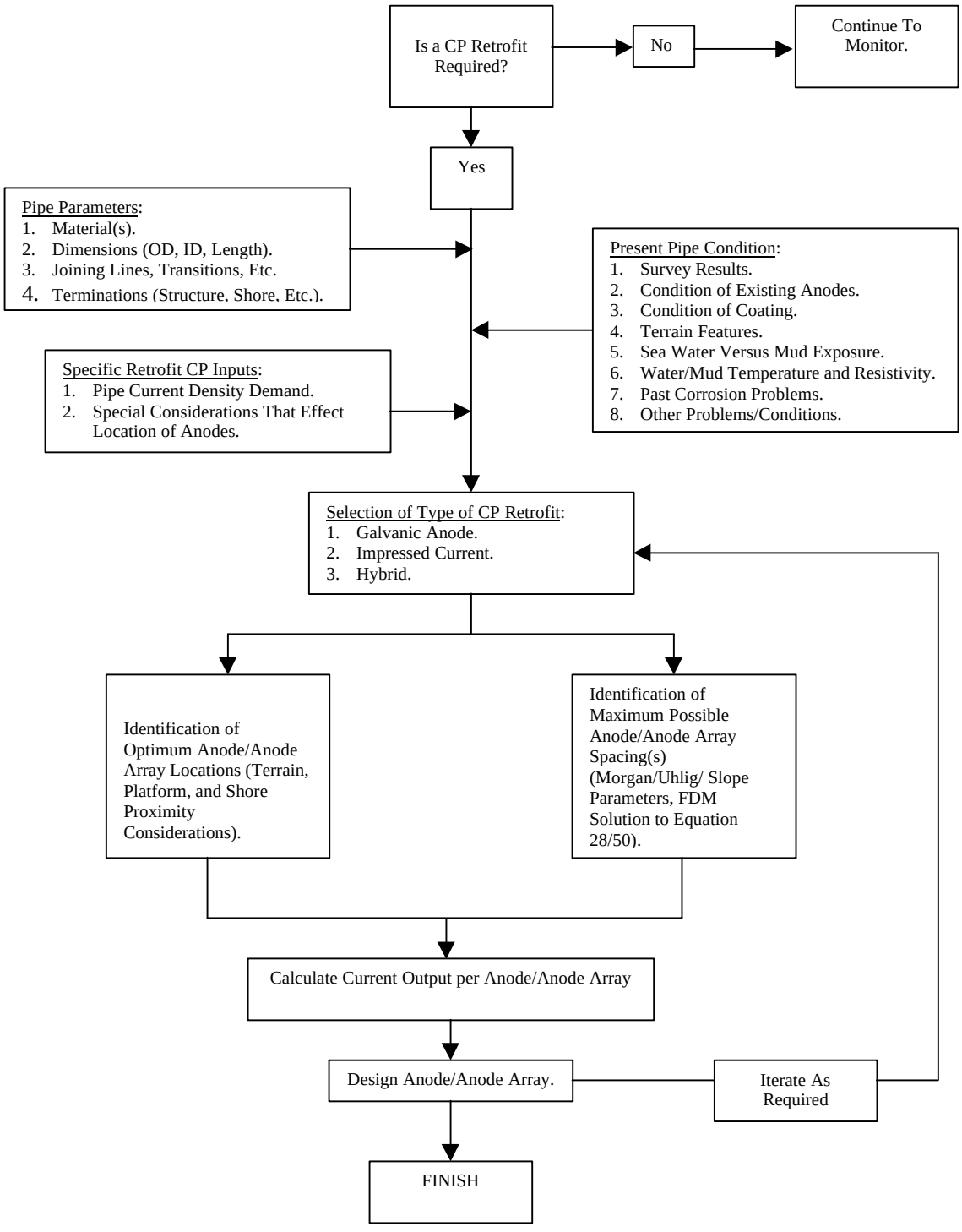

Figure 36: Proposed pipeline retrofit cp flow chart.

BIBLIOGRAPHY

1. T. Andersen and A. Misund, “Pipeline Reliability: An Investigation of Pipeline Failure Characteristics and Analysis of Pipeline Failure Rates for Submarine and Cross-Country Pipelines,” J. Pet. Technology, April, 1983, p. 709.

2. “Analysis of the MMS Pipeline Leaks Report for the Gulf of Mexico, Texaco USA, 133 W. Santa Clara, Ventura, CA 93001, October 25, 1985.

3. J. S. Mandke, “Corrosion Causes Most Pipeline Failures in the Gulf of Mexico, Oil and Gas Journal, October 29, 1990, p. 40.

4. “Improving the Safety of Marine Pipelines,” Committee on the Safety of Marine Pipelines, Marine Board, National Research Council, Washington, D.C., 1994.

5 Minerals Management Service Data Base, Gulf of Mexico Region, New Orleans, LA.

6 C. Weldon and D. Kroon, “Corrosion Control Survey Methods for Offshore Pipelines,” Proceedings International Workshop on Offshore Pipeline Safety, New Orleans, Dec. 4-6, 1991, p. 196.

7. ‘International Workshop on Corrosion Control for Marine Structures,” Eds: G.R.Edwards, W. Hanzalek, S. Liu, D.L. Olson, and C. Smith, Am Bureau of Shipping, Houston, 2000.

8. J. Britton, “Continuous Surveys of Cathodic Protection System performance on Buried Pipelines in the Gulf of Mexico,” paper no. 422 presented at CORROSION/92, Nashville, April 26-30, 1992.

9. "Corrosion Control of Steel-Fixed Offshore Platforms Associated with Petroleum Production", *NACE Standard RP 0176*, NACE, Houston, 1976.

10. “Cathodic Protection Design,” *DnV Recommended Practice RP401*, Det Norske Veritas Industri Norge AS, 1993.

11. "Corrosion Control of Steel-Fixed Offshore Platforms Associated with Petroleum Production", *NACE Standard RP 0176*, NACE, Houston, 1976.

12. Wang, W., Hartt, W. H., and Chen, S., *Corrosion*, vol. 52, 1996, p. 419.

13. W. H. Hartt, Chen, S., and Townley, D. W., *Corrosion*, vol. 54, 1998, p 317.

14. Townley, D. W., “Unified Design Equation for Offshore Cathodic Protection,” paper no. 97473 presented at CORROSION/97, March 9-14, 1997, New Orleans.

15. “Design of Galvanic Anode Cathodic Protection Systems for Offshore Structures,” NACE International Publication 7L198, NACE International, Houston, TX, 1998.

16. Dwight, H. B., *Electrical Engineering*, Vol. 55, 1936, p. 1319.

17. Sunde, E. D., *Earth Conduction Effects in Transmission Systems*, Dover Publications, Inc., New York, 1968.

18. McCoy, J. E., *Transactions Institute of Marine Engineers*, Vol. 82, 1970, p. 210.

19. Cochran, J. C., “A Correlation of Anode-to-Electrolyte Resistance Equations Used in Cathodic Protection,” paper no. 169 presented at CORROSION/82, March 22-26, 1982, Houston.

20. Strommen, R., *Materials Performance*, Vol. 24(3), 1985, p. 9.

21. Cochran, J. C., "Additional Anode-to-Electrolyte Resistance Equations Useful in Offshore Cathodic Protection," paper no. 254 presented at CORROSION/84, April 2-6, 1984, New Orleans.

22. Foster, T., and Moores, V. G., "Cathodic Protection Current Demand of Various Alloys in Sea Water," paper no. 295 presented at CORROSION/86, March 17-2, 1986, Houston.

23. Mollan, R. and Anderson, T. R., "Design of Cathodic Protection Systems," paper no. 286 presented at CORROSION/86, March 17-2, 1986, Houston.

24. Fischer, K. P., Sydberger, T. and Lye, R., "Field Testing of Deep Water Cathodic Protection on the Norwegian Continental Shelf," paper no. 67 presented at CORROSION/87, March 9-13, 1987, San Francisco.

25. Fischer, K. P. and Finnegan, J. E., "Cathodic Protection Behavior of Steel in Sea Water and the Protective Properties of the Calcareous Deposits," paper no. 582 presented at CORROSION/89, April 17-21, 1989, New Orleans.

26. Schrieber, C. F. and Reding, J., "Application Methods for Rapid Polarization of Offshore Structures," paper no. 381 presented at CORROSION/90, April 23-27, 1990, Las Vegas.

27. Burk, J. D., "Dualnode Field Performance Evaluation – Cathodic Protection for Offshore Structures," paper no. 309 presented at CORROSION/91, March 11-14, 1991, Cincinnati.

28. "Pipeline Cathodic Protection – Part 2: Cathodic Protection of Offshore Pipelines," Working Document ISO/TC 67/SC 2 NP 14489, International Standards Organization, May 1, 1999.

29. Morgan, J., *Cathodic Protection*, Macmillan, New York, 1960, pp. 140-143.

30. Uhlig, H. H. and Revie, R. W., *Corrosion and Corrosion Control*, Third Edition, John Wiley and Sons, New York, 1985, p. 223.

31. Strommen, R. and Rodland, A, Materials Performance, Vol. 20 No. 10, 1981, p. 7.

32. McCoy, J. E., "Corrosion Control by Cathodic Protection – Theoretical and Design Concepts for Marine Applications", The Institute of Marine Engineers Transactions, Vol. 82, 1970, p. 210.

33. Chapra, C. S. and Canale, R. P., *Numerical Methods for Engineers*, McGraw-Hill, Second Ed., New York, 1988, pp. 734-737.

34. P. Pierson and W. H. Hartt, "Galvanic Anode Cathodic Polarization of Steel in Sea Water: Part IV – Conductor Arrays on Petroleum Production Platforms," Corrosion, Vol. 55, 1999, p. 686.

APPENDIX A

Derivation of the First-Principles Pipeline Attenuation Equation

Generalized Formulation

Electrode potential (pipe or riser potential in this case), $f_c(z)$, can be represented as the charge gradient associated with a double layer or

$$f_c(z) = U_m(z) - U_e(z) + K_{ref}, \quad \text{(A1}$$

where $U_m(z)$ and $U_e(z)$ are the metallic and electrolyte potentials, respectively, and K_{ref} accounts for the fact that $f_c(z)$ must be measured relative to a reference potential (constant). Also,

$$E_C(z) = f_c(z) - f_{corr}, \quad \text{(A2}$$

where f_{corr} is the free corrosion potential and $E_c(z)$ is the magnitude of polarization. Further, upon taking the second derivative of Equations A1 and A2 and combining,

$$\frac{\partial^2 E_c}{\partial z^2} = \frac{\partial^2 U_m}{\partial z^2} - \frac{\partial^2 U_e}{\partial z^2}. \quad \text{(A3}$$

The approach that was adapted herein was to evaluate Equation A3 by developing expressions for each of the three component terms.

Steady-State Polarization Behavior

Representation of the pipeline or riser polarization in response to the cp current considered that steady-state has been achieved, in which case a constant, unique relationship exists between $f_c(z)$ and cathode current density, $i_c(z)$. Furthermore, the fact that the pipeline is either buried in bottom sediments or is resting on or near the bottom with accumulation of calcareous deposits at bare areas should promote oxygen concentration polarization with a relatively low limiting current density. For simplicity, this polarization behavior is expressed in terms of a linear relationship as

$$f_C(z) = f_{corr} + a \cdot i_c(z), \quad \text{(A4}$$

as shown in Figure 5, where a the polarization resistance.

Pipeline Coating Effects

As noted above, coating of pipelines and risers is necessary for effective, efficient cathodic protection. Because such coatings have typically been field applied at connections and invariably sustain damage during installation, quality in terms of defects and imperfections is generally less than for on-shore counterparts. In the present analysis, the net cathodic current, I_c, upon an area A_c of the pipeline was assumed to conform to the relationship

$$I_c = i_c \cdot A_c = i_s \cdot A_s + i_b \cdot A_b \approx i_b \cdot A_b \,, \qquad \text{(A5}$$

where i_s and i_b are the current densities upon the coated and bare portions of A_c, respectively, and A_s and A_b are the corresponding coated and bare areas. Thus, the relationship

$$i_b \approx i_c \cdot \left(\frac{A_c}{A_b} \right) = i_c \cdot g \,, \qquad \text{(A6}$$

where g is the ratio of the two areas, applies as long as the product of i_b and A_b is much greater than that of i_s and A_s. Accordingly, for the limiting case of bare steel, $A_c = A_b$ and $g = 1$. Alternatively, if the coating is perfect, then A_b is zero and g becomes infinite. Within this context, it should be possible also to relate g to coating conductance. By considering the polarizing current as occurring on bare steel alone, Equation 4 can be reformulated as

$$f_C(z) = f_{corr} + a \cdot i_b(z) = f_{corr} + (a \cdot g) \cdot i_c(z); \qquad \text{(A7}$$

and from Equation A2 it follows that

$$E_C(z) = (a \cdot g) \cdot i_c(z), \qquad \text{(A8}$$

whereby polarization is expressed in terms of current density, coating quality, and polarization resistance.

Electrolyte Potential Variation

To develop an expression for U_e, consider a pipeline that is protected galvanically by a spherical anode of radius r_a located at the origin, as shown schematically in Figure A1. The anode discharges a total current I_a into the electrolyte, and this results in a cathodic current density $i_c(z)$ on the pipe at z. Correspondingly, the net current entering a pipe element of length dz, $dI_c(z)$, is

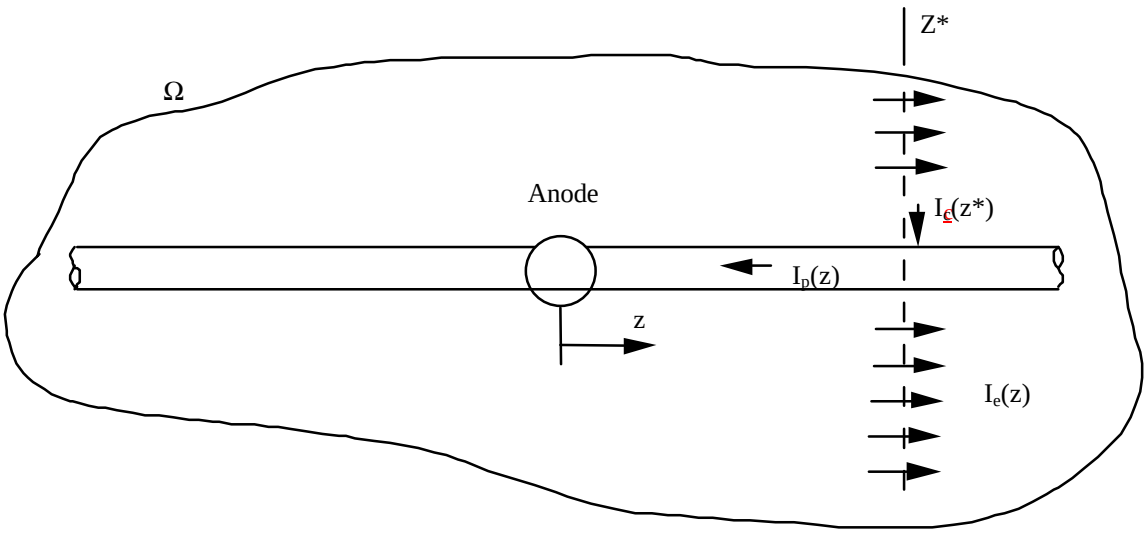

Figure A1: Current field and individual current components associated with a galvanic anode upon a pipe.

$$dI_c(z) = 2\pi r_p \cdot dz \cdot i_c(z). \qquad \text{(A9}$$

Further, let r be a point in the electrolyte directly above the differential cathode element at z and sufficiently close to the pipe that current density in the y-direction at r is $i_c(z)$. From the classical equation for the potential drop associated with a spherical electrode in an electrolyte of resistivity r_e, the potential difference between points r_1 and r_2, $\Delta f_{r_1 \to r_2}$, is given by,

$$Df_{r_1 \to r_2} = -\int_{r_1}^{r_2} b_e \, dn = -\int_{r_1}^{r_2} \frac{r_e I}{4\pi r^2} dr = \frac{r_e I}{4\pi} \cdot \left[\frac{1}{r_1} - \frac{1}{r_2} \right], \qquad \text{(A10}$$

where b_e is the electric field intensity and I is the total current leaving the source (anode). For the case of a spherical anode of radius r_a superimposed upon a pipeline, the potential difference between the anode surface and a radial outward distance $r = z$, $Df_{r_a \to z}$, is

$$Df_{r_a \to z} = \frac{r_e I}{4\pi} \left[\frac{1}{r_a} - \frac{1}{z} \right]; \qquad \text{(A11}$$

and the corresponding resistance between these two points, $R_e(z)$, is

$$R_e(z) = \frac{r_e}{4\pi} \cdot \left[\frac{1}{r_a} - \frac{1}{z} \right]. \qquad \text{(A12}$$

Correspondingly,

$$\frac{\partial}{\partial z}\left[R_e(z)\right] = \frac{r_e}{4\pi z^2}. \qquad \text{(A13}$$

Application of the above equations to the present situation assumes that 1) the coating on the pipeline or riser is of sufficient quality that the metallic pipe does not significantly perturb the spherical symmetry of the current field generated by the anode and 2) current density on the pipe is sufficiently small that the *IR* drop at this electrode is negligible (see Figure A1).

Consider now the enclosed surface *W* in Figure A1 that encompasses the anode and a sufficient length of the pipeline such that the entire current field is maintained within it. For the case of multiple, equally spaced anodes, this surface intersects the pipeline at $z = L$, where $2L$ is the spacing between anodes. Conservation of charge requires that the net current passing through a planar surface perpendicular to the pipeline at $z = z^*$, $I_e(z^*)$, conform to the expression

$$I_e(z^*) = I_p(z^*) = \int_{z^*}^{L} 2\pi r_p \cdot i_C(z)\,dz, \qquad \text{(A14}$$

where $I_p(z^*)$ is the net current returning to the anode through the pipe at $z = z^*$ or, alternatively, the total current entering the pipe from the electrolyte between z^* and L; and $i_c(z^*)$ is the cathode current density. The net current in the electrolyte (anode current, $I_a(z^*)$) at $z=z^*$ is equal to the contribution from $I_e(z^*)$ from both sides of the anode or

$$I_a(z^*) = 2I_p(z^*) = 2\int_{z^*}^{L} 2\pi r_p \cdot i_c(z^*)\,dz. \qquad \text{(A15}$$

Also, the change in net current in the *z*-direction of the pipe across *dz* is equal to one-half the change in net anode current in the electrolyte or,

$$\frac{\partial}{\partial z}\left[I_a(z)\right] = 2\cdot\frac{\partial}{\partial z}\left[I_p(z)\right] = -4\pi r_p \cdot i_c(z), \qquad \text{(A16}$$

where $I_p(z)$ is negative and $I_a(z)$ and $i_c(z)$ are both positive by convention. Upon combining with Equation 15, the latter expression becomes

$$\frac{\partial}{\partial z}[I_a(z)] = -\frac{4pr_p}{ag} \cdot E_c(z). \qquad \text{(A17}$$

Consider that U_e^a and $U_e^c(z)$ are the electrolyte potentials at the anode and pipeline surfaces, respectively, where the latter is a function of and the former is independent of *z*, such that the potential difference between the anode and cathode at *z*, $DU_e(z)$, is given by,

$$DU_e(z) = U_e^a - U_e^c(z). \qquad \text{(A18}$$

Accordingly, the potential gradient along the pipe may be expressed as,

$$\frac{\partial U_e}{\partial z} = -\frac{\partial}{\partial z}[DU_e(z)] = -\frac{\partial}{\partial z}\left[U_e^a - U_e^c(z)\right] = -\frac{\partial}{\partial z}\left[-U_e^c(z)\right]. \qquad \text{(A19}$$

Then, from Equations A8, 19, A17, and A19,

$$\frac{\partial U_e(z)}{\partial z} = \frac{\partial}{\partial z}[I_a(z) \cdot R_e(z)] = \frac{\partial}{\partial z}[I_a(z)] \cdot R_e(z) + I_a(z) \cdot \frac{\partial}{\partial z}[R_e(z)] =$$

$$\frac{r_e \cdot r_p}{ag} \cdot E_c(z) \cdot \left[\frac{1}{r_a} - \frac{1}{z}\right] + \frac{r_e \cdot r_p}{ag \cdot \cdot z^2} \int_z^L E_c(z)dz \qquad \text{(A20}$$

and

$$\frac{\partial^2 U_e}{\partial z^2} = \frac{r_e \cdot r_p}{ag} \cdot \left[\left(\frac{1}{r_a} - \frac{1}{z}\right)\right] \cdot \frac{\partial E_c(z)}{dz} + \frac{2E_c(z)}{z^2} - \frac{2}{z^3} \cdot \int_z^L E_c(z)dz. \qquad \text{(A21}$$

Metallic Pipe Potential Variation

The potential gradient in the *z*-direction within the pipe, $\frac{\partial U_m}{\partial z}$, can be represented in terms of the resistance per unit length, R_m, as given by

$$R_m = \frac{r_m}{A_p}, \qquad \text{(A22}$$

where r_m is the metal resistivity and A_p is the cross sectional area of the pipe. The change in the pipe return current, $I_p(z)$, per unit length at z is equal to the total current entering the pipe at z or

$$\frac{\partial I_p(z)}{\partial z} = -2p \cdot r_p \cdot i_c(z), \qquad \text{(A23}$$

where r_p is the outer pipe radius. By Ohm's law, the potential change along the pipe is given by

$$\frac{\partial U_m}{\partial z} = -R_m \cdot I_p(z). \qquad \text{(A24}$$

Correspondingly, differentiation of this expression and combining with Equations A8 and A23 yields

$$\frac{\partial^2 U_m}{\partial z^2} = \frac{R_m \cdot 2p \cdot r_p}{a \cdot g} \cdot E_c(z). \qquad \text{(A25}$$

The Governing Equation

Substitution of the appropriate expressions that contain the electrolytic and metallic potential gradients along the pipeline (Equations A21 and A25) into Equation A3 and combining and grouping terms provides an expression of potential attenuation along a pipeline or riser as,

$$\frac{\partial^2 E_c(z)}{\partial z^2} + \frac{\partial E_c(z)}{\partial z} \cdot H \cdot \left(\frac{1}{r_a} - \frac{1}{z}\right) + E_c(z) \cdot \left(\frac{2H}{z^2} - B\right) = 2H \cdot \frac{1}{z^3} \cdot \int_z^L E\left(z^*\right) dz^* \qquad \text{(A26}$$

where

$$H = \frac{r_e \cdot r_p}{ag} \text{ and}$$

$$B = \frac{R_m \cdot 2pr_p}{ag}.$$

APPENDIX B

Spacing Distance between Crossing Pipelines

As part of the present research project, appropriateness of the present MMS regulation that requires a minimum separation distance of 18 inches between crossing marine pipelines has been addressed. In this regard, it is projected that any one of several factors could potentially impact the effect that one pipeline might have upon a second in the vicinity of where they cross. These include, but are not necessarily limited to, 1) miscalculations and uncontrollable occurrences during installation of the crossing pipeline, 2) settlement of one pipeline upon the other with time, and 3) loading of one pipeline by the other in conjunction with a storm or mudslide. From the standpoint of corrosion, the sole question of significance is whether the cathodic protection system of one line might affect the corresponding system and corrosion upon the other. Thus, if the pipelines share a common electrical ground and if one is polarized to a more negative potential (receives greater cathodic protection) than the other, then it can be reasoned that a positive direct current (stray current) could discharge from the former (more negatively polarized pipeline) to the latter (less polarized pipeline). While discharge of positive current from metal into an electrolyte normally results in corrosion (stray current corrosion), such attack should not occur as long as potential for both lines in negative to –0.80 $V_{Ag/AgCl}$. In actuality, such discharge would be from the anode(s) of one pipeline to the other pipeline to an extent that the polarized potential of each approaches the same value. This potentially could cause premature depletion of anodes on the one pipeline. However, such an occurrence should not be affected by separation distance at a point of crossing. In cases where the cathodic protection system on each line is of the galvanic (sacrificial) anode type, as is normally the case, any interactions as alluded to above should not be of significance because of 1) the low driving voltage involved, 2) polarization resistance of the pipeline steel, and 3) the fact that electrical resistivity of steel is about six orders of magnitude less than that of sea water. For this same reason, occurrence of an exceptionally low sea water resistivity, as might occur in conjunction with an eroding salt dome, should be inconsequential. If, however, the cathodic protection system on one or both pipelines is of the impressed current type, then it is possible that negative effects in the form of stray current corrosion could result on one or both of the lines. It is highly unlikely, however, that such corrosion would be influenced by pipeline separation distances that typically exist at a point of crossing (several inches to several feet).